

1

2

Figure TFIELD-34. Observed Drawdowns for the H-11 Hydraulic Test

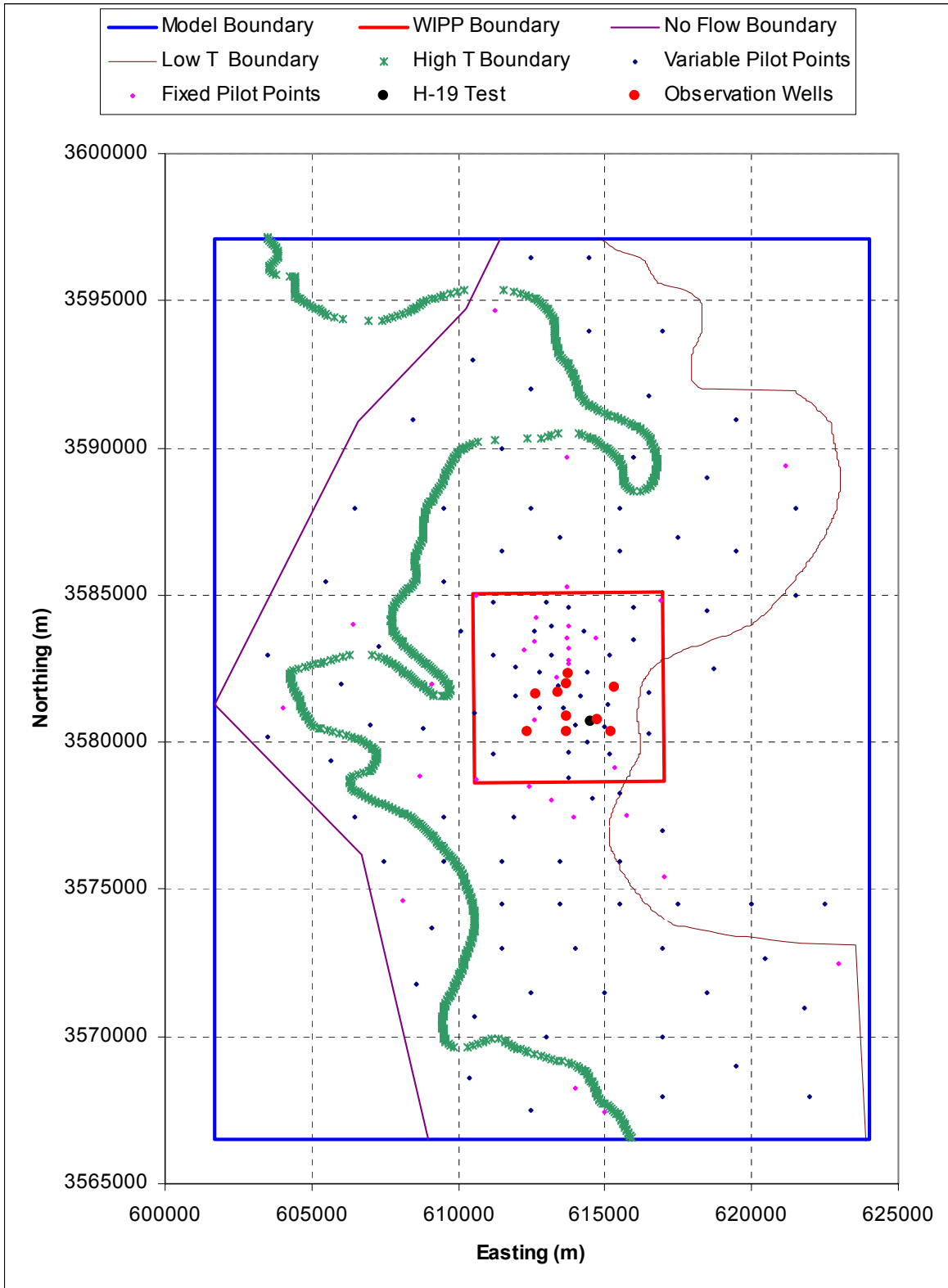
3 The number of measurements used for calibration that were made at individual wells during
 4 individual tests ranged from 6 to 104, and the number of measurements used for calibration that
 5 were made at all wells during a single test ranged from 64 to 410. This means that different well
 6 responses and different tests carried different cumulative weights. The spatially broadest sampling
 7 of transient data possible was used in an effort to get transient coverage of as much of the modeling
 8 domain as possible. In those areas where no transient data are available, the calibration is
 9 dominated by fitting the model to the steady-state measurements. The greatest coverage of
 10 transient data is within the boundaries of the WIPP site, which is also the area of most significance
 11 for radionuclide transport.

12 The maximum observed drawdown, the weight assigned to all the observed test values for each
 13 test, and the total number of observations for each observation well are given in Table
 14 TFIELD-10.

15 ***TFIELD-6.8 Assignment of Pilot Point Geometry***

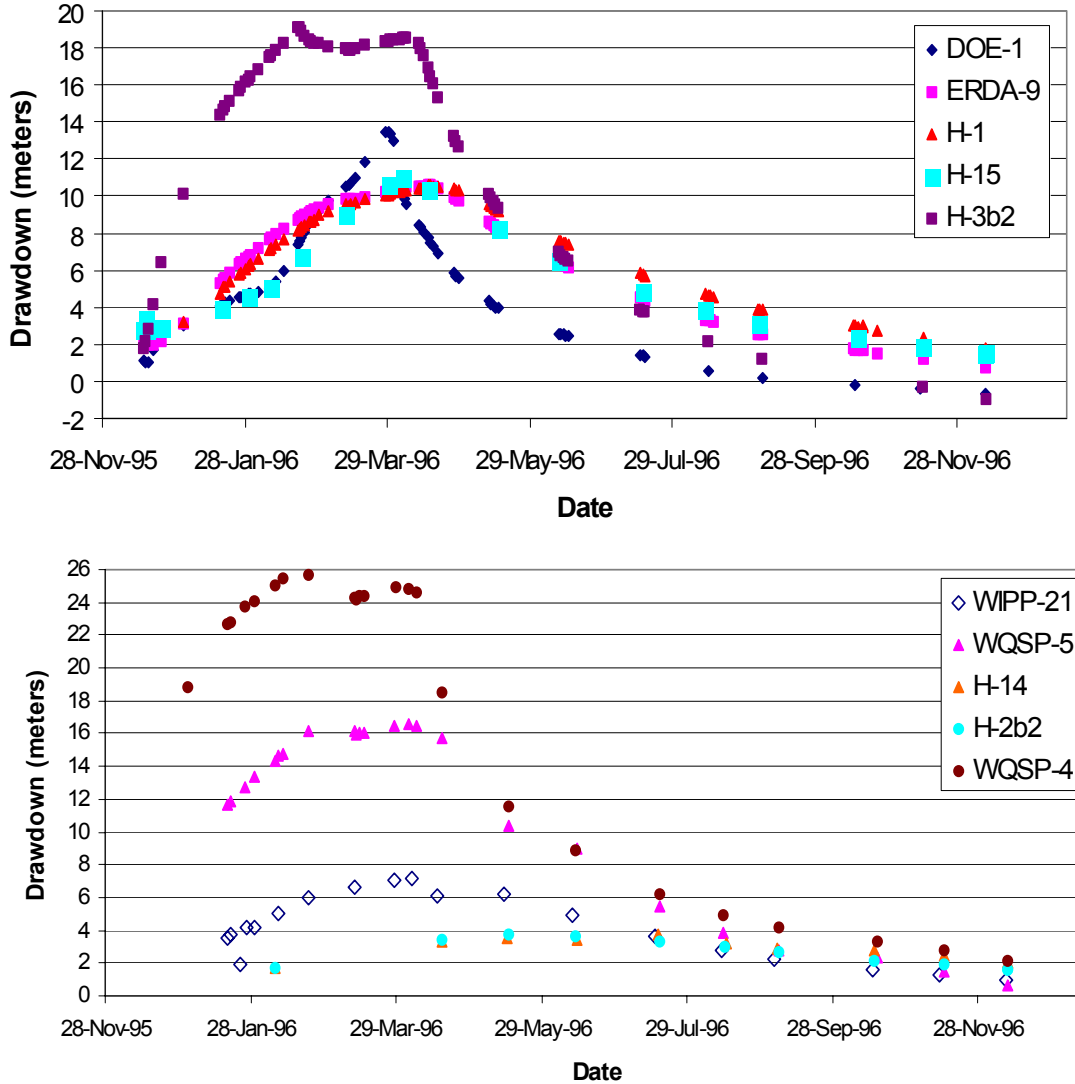
16 A major development in the field of stochastic inverse modeling that has occurred since the T
 17 fields were constructed for the CCA in 1996 is that inverse techniques are now capable of
 18 simultaneously determining optimal T values at a large number of pilot points. In the T fields
 19 constructed for the CCA, pilot points were added one at a time and each point was calibrated
 20 prior to the addition of the next pilot point. Furthermore, the total number of pilot points was
 21 limited to less than or equal to the total number of T observations to avoid numerical instabilities
 22 in the solution of the inverse problem. With the techniques now available and implemented in
 23 PEST, it is possible to use many more pilot points than there are T observations and to calibrate
 24 these pilot points simultaneously.

25 The pilot-point locations were chosen using a combination of a regular grid approach and
 26 deviations from that grid to accommodate specific pumping- and observation-well locations



1
2
3

Figure TFIELD-35. Locations of the H-19 Hydraulic Test Well and Observation Wells



1
2 **Figure TFIELD-36. Observed Drawdowns From the H-19 Hydraulic Test**

3 (Figure TFIELD-38). The goal in these deviations from the regular grid was to put at least one
 4 pilot point between each pumping well and each of its observation wells. Details of the pilot-
 5 point locations relative to the pumping and observation wells in the WIPP site area are shown in
 6 Figure TFIELD-39. This combined approach of a regular grid with specific deviations from that
 7 grid follows the guidelines for pilot-point placement put forth by John Doherty (the author of
 8 PEST) as Appendix 1 in the work of McKenna and Hart (2003a). Pilot points located at the T
 9 measurement locations were held as fixed values during the optimization (fixed pilot points
 10 shown as magenta squares in Figure TFIELD-38). The variable pilot points (dark blue diamonds
 11 in Figure TFIELD-38) are those where the T value was adjusted during the calibration
 12 procedure. A total of 43 fixed and 100 variable pilot points was used in the T-field calibration
 13 process. The zone option in PEST was employed to limit the influence of pilot points in any one
 14 zone (e.g., high T or low T) to adjusting only locations that are in the same zone.

Table TFIELD-9. Discretization of Time into 29 Stress Periods and 127 Time Steps with Pumping Well Names and Pumping Rates

Event Name	Global Stress Period No.	Internal Stress Period No.	Stress Period Length (s)	No. of Time Steps	Start Date	Stop Date	Pumping Well(s)	Pumping Rate(s) (m ³ /s)
Steady	1	1	86400	1	10/14/859:00	10/15/859:00	0	0
H-3	2	1	5356800	8	10/15/859:00	12/16/859:00	H-3	3.03E-04
	3	2	10892700	8	12/16/859:00	4/21/8610:45	None	0.00E+00
	4	3	22976100	1	4/21/8610:45	1/12/879:00	None	0.00E+00
WIPP-13	5	1	3110400	8	1/12/879:00	2/17/879:00	WIPP-13	1.89E-03
	6	2	7539900	8	2/17/879:00	5/15/8715:25	None	0.00E+00
	7	3	55359360	1	5/15/8715:25	2/14/899:01	None	0.00E+00
P-14	8	1	44928	3	2/14/899:01	2/14/8921:29	P-14	3.92E-03
	9	2	174612	8	2/14/8921:29	2/16/8922:00	P-14	3.64E-03
	10	3	50400	3	2/16/8922:00	2/17/8912:00	P-14	3.37E-03
	11	4	1820396	8	2/17/8912:00	3/10/8913:39	None	0.00E+00
	12	5	193212124	1	3/10/8913:39	4/24/95 19:42	None	0.00E+00
H-19	13	1	148860	1	4/24/9519:42	4/26/95 13:03	H-19b0	2.26E-04
	14	2	4399020	1	4/26/9513:03	6/16/9511:00	None	0.00E+00
	15	3	3614400	1	6/16/9511:00	7/28/95 7:00	H-19b0	2.36E-04
	16	4	1168200	1	7/28/95 7:00	8/10/95 19:30	None	0.00E+00
	17	5	1292700	1	8/10/9519:30	8/25/9518:35	H11	2.44E-04
	18	6	9651300	1	8/25/9518:35	12/15/9511:30	None	0.00E+00
	19	7	2878200	8	12/15/9511:30	1/17/9619:00	H-19b0	2.71 E-04
	20	8	670680	3	1/17/9619:00	1/25/9613:18	H-19b0	2.52E-04
	21	9	238980	3	1/25/9613:18	1/28/96 7:41	H-19b0, WQSP-1	2.52E-04, 4.30E-04
	22	10	872340	3	1/28/96 7:41	2/7/9610:00	H-19b0	2.52E-04
	23	11	1047000	8	2/7/9610:00	2/19/9612:50	H-19b0, H-11	2.52E-04, 2.23E-04
	24	12	81600	3	2/19/9612:50	2/20/9611:30	H-19b0, H-11	1.55E-04, 2.23E-04
	25	13	345600	3	2/20/96 11:30	2/24/9611:30	H-19b0, H-11, WQSP-2	1.55E-04, 2.23E-04, 4.5E-04
	26	14	1395000	8	2/24/96 11:30	3/11/9615:00	H-19b0, H-11	1.55E-04, 2.23E-04
	27	15	1445100	8	3/11/9615:00	3/28/96 8:25	H-19b0, H-11	1.55E-04, 3.76E-04
	28	16	1220700	8	3/28/96 8:25	4/11/9611:30	H-19b0	1.55E-04
	29	17	21074400	8	4/11/9611:30	12/11/969:30	None	0.00E+00

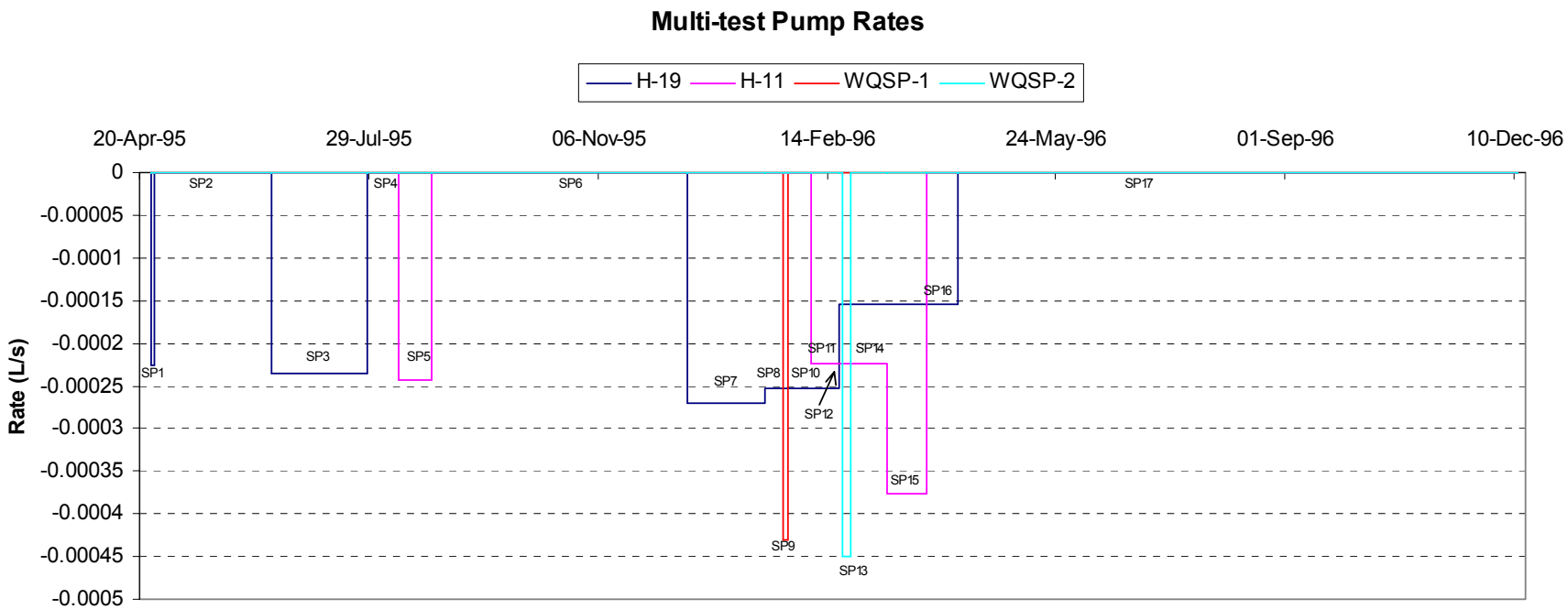


Figure TFIELD-37. Temporal Discretization and Pumping Rates for the Fifth Call to MODFLOW-2000. A total of 17 stress periods (SPs) are used to discretize this model call.

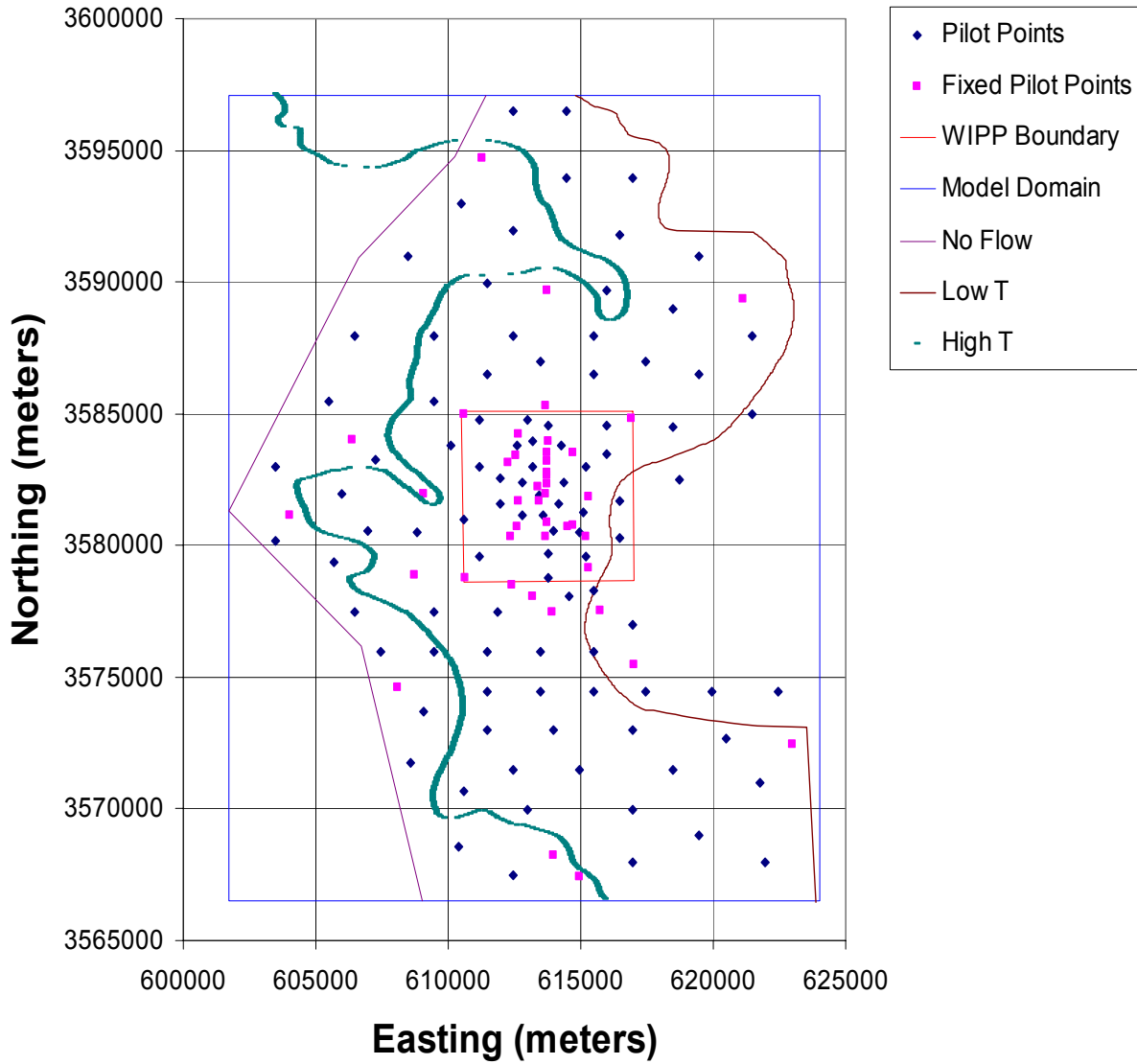
1

Table TFIELD-10. Observation Weights for Each of the Observation Wells

Test Well Observation Well	Maximum Drawdown (m)	Weight	Number of Observations
Steady	NA	2.273	35
H3-DOE1	5.426	0.184	57
H3-H1	10.396	0.096	26
H3-H11b1	3.622	0.276	19
H3-H2b2	3.781	0.265	20
W13-DOE2	12.138	0.082	104
W13-H2b2	0.781	1.281	23
W13-H6	5.545	0.180	93
W13-P14	0.570	1.755	38
W13-W12	1.553	0.644	27
W13-W18	6.481	0.154	26
W13-W19	5.048	0.198	22
W13-W25	0.246	4.062	11
W13-W30	3.391	0.295	24
P14-D268	0.432	2.317	38
P14-H18	0.113	8.850	21
P14-H6b	0.701	1.427	21
P14-W25	0.432	2.315	22
P14-W26	0.137	7.310	20
WQSP1-H18	1.431	0.699	47
WQSP1-W13	1.260	0.794	47
WQSP1-WQSP3	0.000	20.000	25
WQSP2-DOE2	1.178	0.849	34
WQSP2-H18	0.529	1.892	35
WQSP2-W13	1.053	0.949	34
WQSP2-WQSP1	1.132	0.884	6
WQSP2-WQSP3	0.000	20.000	18
H11-H17	1.030	0.971	23
H11-H4b	0.232	4.317	11
H11-H12	0.033	20.190	11
H11-P17	1.628	3.304	19
H19-DOE1	13.463	0.074	70
H19-ERDA9	10.571	0.095	80
H19-H1	10.618	0.094	80
H19-H15	11.110	0.090	22
H19-H3b2	19.283	0.052	69
H19-W21	7.153	0.140	19
H19-WQSP5	16.623	0.060	24
H19-H14	3.759	0.602	11
H19-H2b2	3.794	0.608	11
H19-WQSP4	25.721	0.462	24

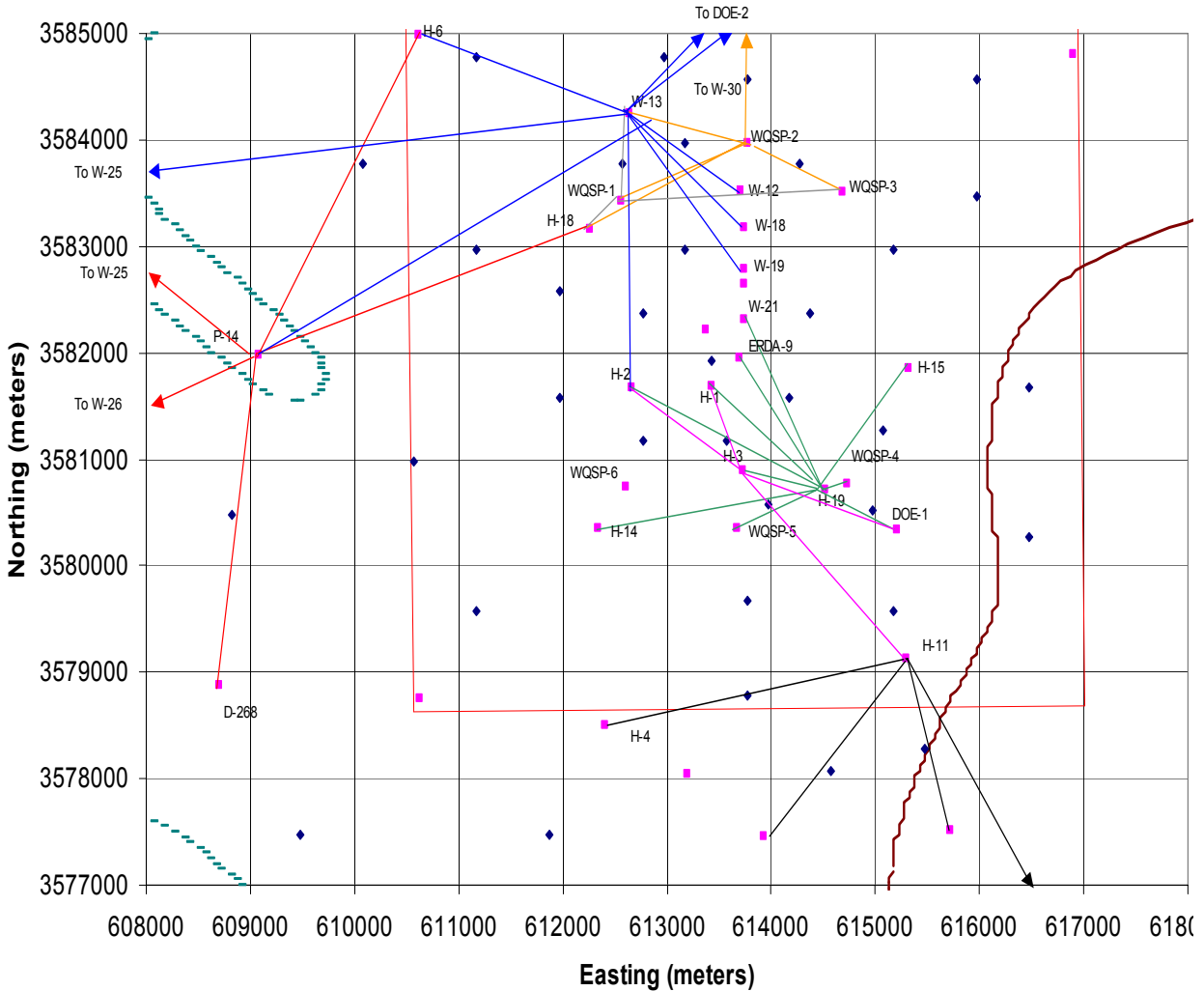
2

3



1
2
3

Figure TFIELD-38. Locations of the Adjustable and Fixed Pilot Points Within the Model Domain



1
 2 **Figure TFIELD-39. Close-Up View of the Pilot-Point Locations in the Area of the WIPP**
 3 **Site. The colored (solid) lines connect the pumping and observation wells. The legend for**
 4 **this figure is the same as that for Figure TFIELD-38.**

5 The variogram model for the residuals between the T measurements and the base field has a
 6 range of 1,050 m (3,445 ft). Because the pilot-point approach to calibration uses this range as a
 7 radius of influence, locations of the adjustable pilot points were as much as possible set to be at
 8 least 1,050 m (3,445 ft) away from other pilot points (adjustable or fixed). For maximum
 9 impact, all pilot points should be at least 2,100 m (6,890 ft) away from any other pilot point but,
 10 given the existing well geometry, this distance was not always achievable.

11 ***TFIELD-6.9 Stochastic Inverse Calibration***

12 The seed realizations are input to the inverse model using the pilot-point method. The seed
 13 realizations are calibrated to the steady-state and transient head measurements. The residuals
 14 and the T-field calculations are done in log₁₀ space so that a unit change in the residual equates to
 15 a one order of magnitude change in the value of T. The initial values of the pilot points are equal

1 to the value of the initial residual field at each pilot-point location. The pilot points are
 2 constrained to have a maximum perturbation of ± 3.0 from the initial value except for those pilot
 3 points within the high-T zone in Nash Draw (Figure TFIELD-11) and the low-T zone on the
 4 eastern side of the model domain that are limited to perturbations of ± 1.0 . These limits are
 5 employed to maintain the influence of the geologic conceptual model on the calibrated T fields.

6 Figure TFIELD-11 is updated as Figure TFIELD-40 to show, conceptually, how the addition of
 7 two pilot points along the cross section can modify the residual field and then update the T field.
 8 The pilot points are shown as the open circles in Figure TFIELD-40 and are used to modify the
 9 residual field before it is added to the base T field. Compare the shape of the dashed red and blue
 10 lines in Figure TFIELD-40 to the same lines in Figure TFIELD-11. The values of the residuals at
 11 the observation points are held fixed so any adjacent pilot points cannot modify them.

12 At the heart of the calibration process is the iterative adjustment of the residual field at the pilot
 13 points by PEST and the subsequent updates of the residual field at the locations surrounding the
 14 pilot points based on the shape of the variogram modeled on the raw residuals. The updated
 15 residual field is then combined with the base T field (see Figure TFIELD-18) and then used in
 16 MODFLOW-2000 to calculate the current set of modeled heads. These modeled heads are then
 17 input to PEST for the next iteration.

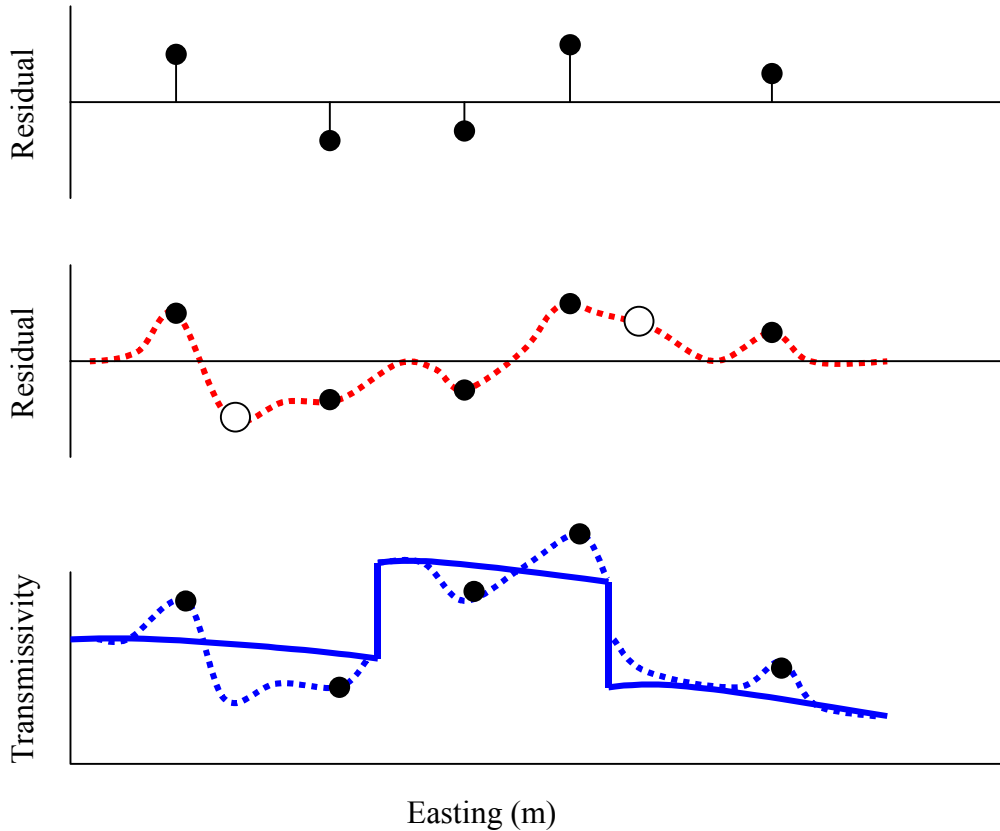
18 The objective function minimized by PEST (ϕ) is a combination of the weighted sum of the
 19 squared residuals between the measured and observed steady-state head data, the weighted sum
 20 of the squared residuals between the measured and observed transient drawdown data, and the
 21 weighted sum of the squared differences in the estimated T value between pairs of pilot points.

22 ϕ is defined as:

$$23 \quad \phi = \sum_{i=1}^{n_{obs}^{SS}} (W_i^{SS} (H_i^{obs-SS} - H_i^{calc-SS}))^2 + \sum_{i=1}^{n_{wells}^{Tr}} \sum_{j=1}^{n_{obs}^{Tr}} (W_i^{Tr} (D_j^{obs-Tr} - D_j^{calc-Tr}))^2 + \sum_{i=1}^{n_{PP}} \sum_{j=j}^{n_{PP}} W_{ij}^R (PP_i - PP_j) \quad (9)$$

24 where n_{obs} is the number of head observations, n_{wells} is the number of wells, n_{PP} is the number of
 25 pilot points, W is the weight assigned to a group of measurements, H^{obs} and H^{calc} are the values
 26 of the observed and calculated heads, respectively, D^{obs} and D^{calc} are the values of the observed
 27 and calculated drawdowns, respectively, PP refers to the \log_{10} T value at a pilot point, and
 28 superscripts SS , Tr , and R refer to steady-state measurements, transient measurements, and pilot-
 29 point regularization, respectively. For this work, the weights on the head and drawdown
 30 observations are as given in Table TFIELD-10. The third weighted sum of squares in the
 31 objective function is the regularization portion of the objective function. This weighted sum of
 32 squares involves the difference in T values between each pair of pilot points ($PP_i - PP_j$) and is
 33 designed to keep the T field as homogeneous as possible and to provide numerical stability when
 34 estimating more parameters than there are data. The pilot-point regularization weights, W_{ij}^R , are
 35 defined by the kriging factors and are a function of the distance between any two pilot points.

36 The stochastic inverse calibration process uses multiple pre- and post-processor codes in addition
 37 to PEST and MODFLOW-2000. The overall numerical approach to the T-field calibration is
 38 shown in Figures TFIELD-41 and TFIELD-42 and the details on this approach are documented
 39

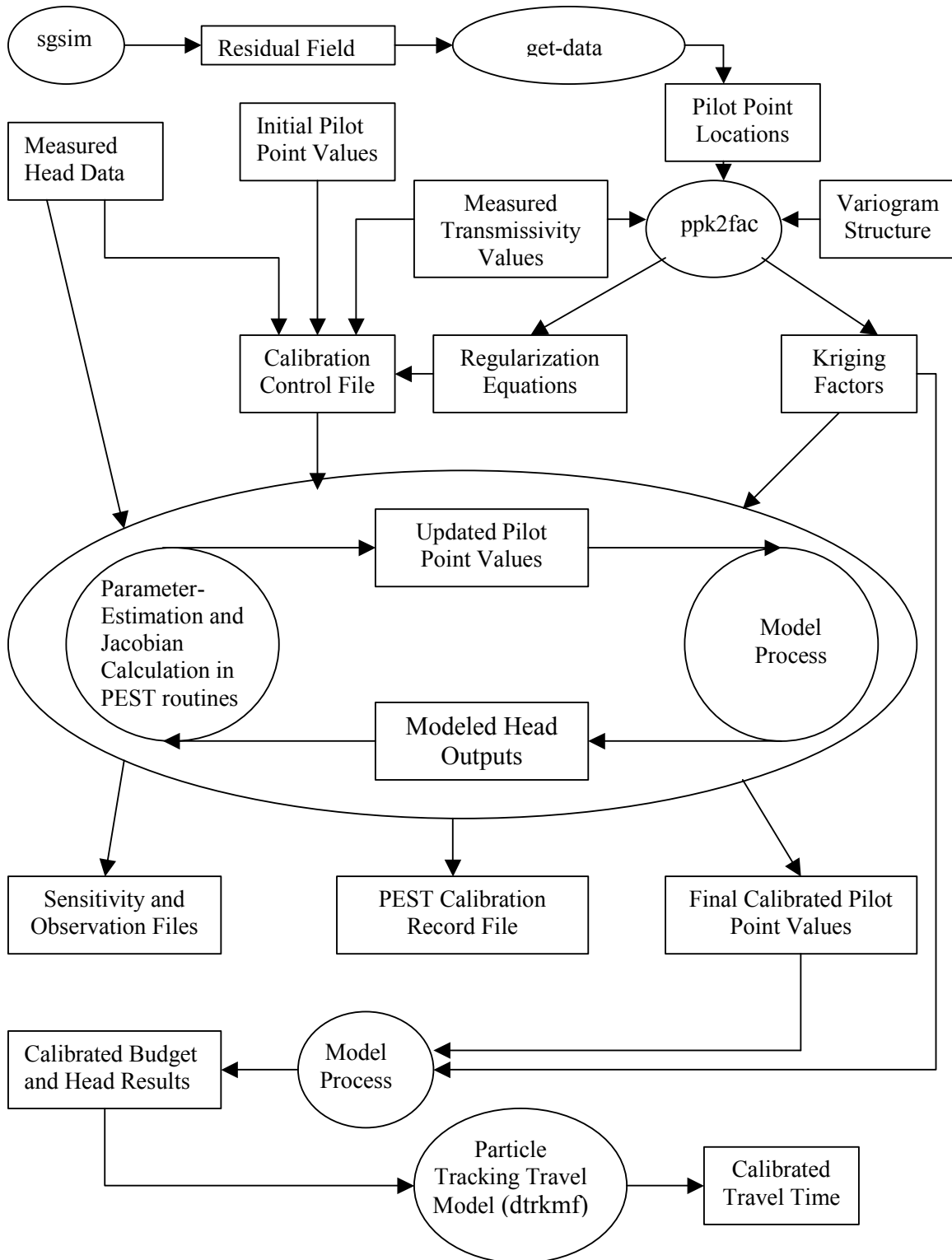


1
 2 **Figure TFIELD-40. Conceptual Cross-Section Showing the Addition of Pilot Points to the**
 3 **Optimization Process**

4 in McKenna and Hart (2003a, 2003b). The top of Figure TFIELD-41 shows the pre-processing
 5 steps. The large oval in the middle of the figure contains the link between MODFLOW-2000
 6 and PEST. The “model process” portion of the figure is expanded and the details are shown in
 7 Figure TFIELD-42. The output files and the connection to the particle-tracking code are shown
 8 in the bottom of Figure TFIELD-41.

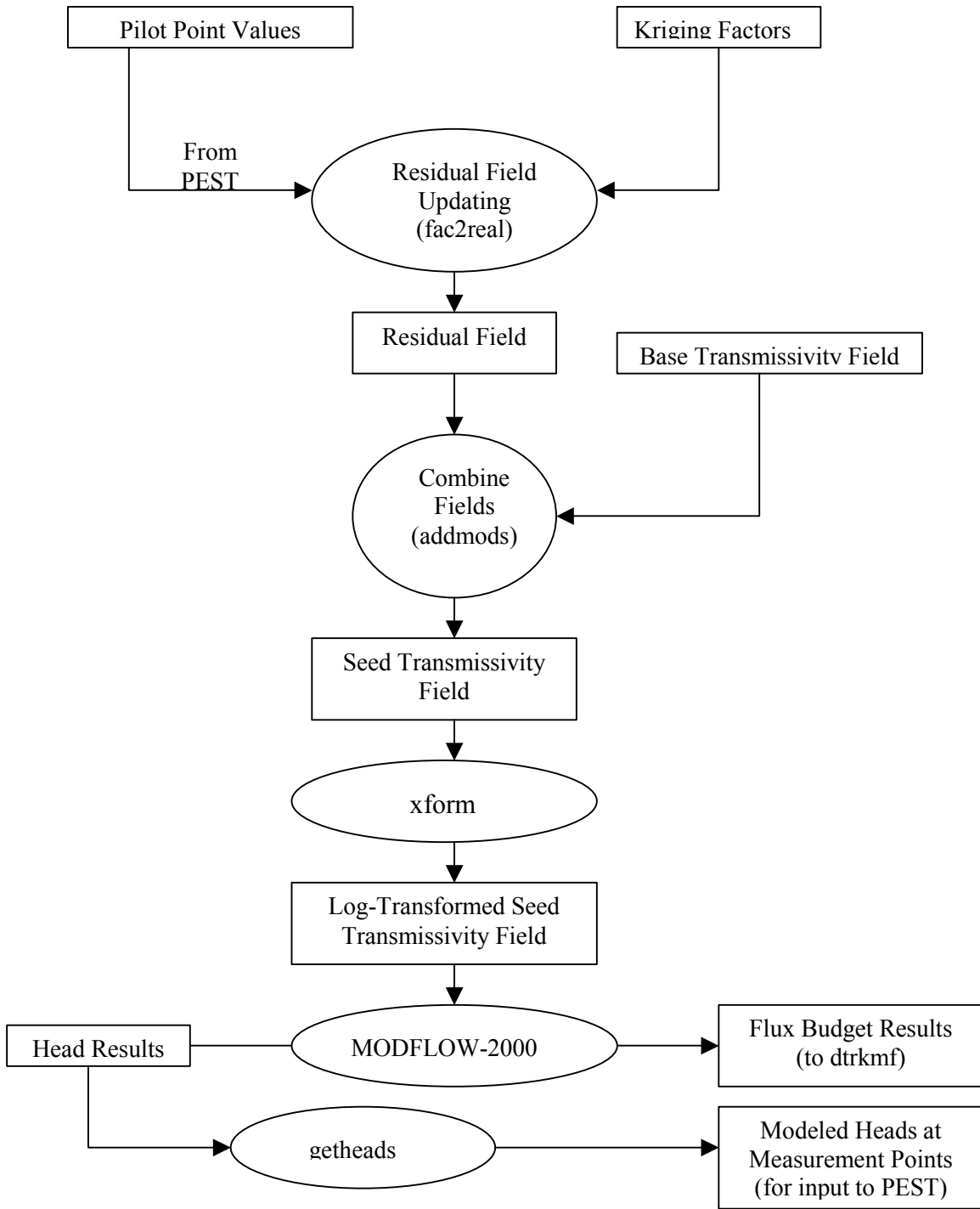
9 The calibration process is run iteratively until at least one of three conditions are met: (1) the
 10 number of iterations reaches the maximum allowable number of 15; (2) the objective function
 11 reaches a predefined minimum value of 1,000 m²; or (3) the value of the objective function
 12 changes by less than one percent across three consecutive iterations.

13 At the end of the calibration process, a residual field is created that when added to the base T
 14 field reproduces the measured T values at the 43 measurement locations and provides a
 15 minimum sum of squared errors (SSE) between the observed and model-predicted
 16 heads/drawdowns. An example of the final step in the creation of a calibrated T field is shown in
 17 Figure TFIELD-43. The computational cost of calibrating to the multiple transient events is
 18 significant. For comparison, a single forward run of MODFLOW-2000 in steady-state takes on
 19 the order of 10-15 seconds on a 1.9-GHz Athlon processor, whereas the run time for the
 20 combined steady-state and transient events is approximately three minutes (a factor of 12-18
 21 times longer).



1
2
3

Figure TFIELD-41. Flow Chart of the Stochastic Inverse Calibration Process Used to Create the Final Calibrated Transmissivity Fields



1
2
3

Figure TFIELD-42. Flow Chart of the Core of the Inversion Process Highlighting the Connection Between PEST and MODFLOW-2000

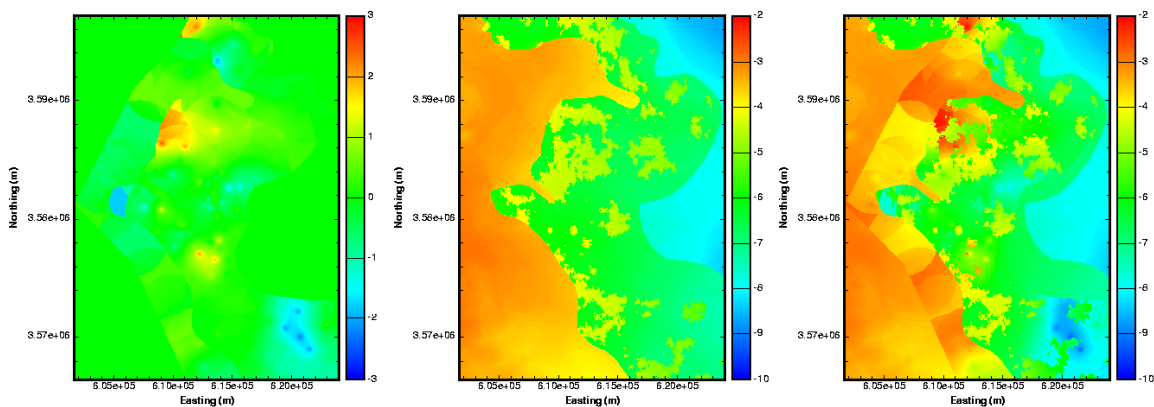


Figure TFIELD-43. Example Final Steps in the Creation of a Calibrated T Field. The calibrated residual field (left image) is added to the base T field (middle image) to get the final calibrated T field (right image). All color scales are in units of $\log_{10} T$ (m^2/s).

Due to these longer run times, two separate parallel PC clusters were employed. Each of these clusters consists of 16 computational nodes running 1.9-GHz Athlon processors with 1 gigabyte of RAM. One cluster is located in Albuquerque, NM and the other is in the Sandia office in Carlsbad, NM. Both clusters use the Linux operating system. The total number of forward runs necessary to complete the calibration process can be estimated as:

$$\text{Total Runs} \cong (\# \text{ of parameters}) \times (\# \text{ of PEST iterations}) \times (\text{average runs per iteration}) \times (\# \text{ of base T fields}).$$

The maximum number of iterations used in these runs was set to 15, although not all fields went to the maximum number of iterations. Additionally, on average for the first four iterations, PEST used forward derivatives to calculate the entries of the Jacobian matrix and each entry only required a single forward model evaluation. For the remaining 11 iterations, PEST used central derivatives to calculate the Jacobian entries and each calculation required two forward evaluations of the model (22 total). The average number of model evaluations is $1.733 = [(4 + 22)/15]$. Therefore an estimate of the maximum possible total number of forward runs is equal to: $100 \text{ pilot points} \times 15 \text{ iterations/field} \times 1.73 \text{ runs/iteration} \times 150 \text{ T fields} = 390,000 \text{ runs}$. The total time necessary to complete these calculations in serial mode on a single processor would be 813 days, or 2.22 years. PEST allows for parallel calculation of the Jacobian matrix, and this option was used to decrease the total run time significantly relative to the time needed for serial computation.

The model run times, as well as the time necessary to read and write input/output files across the cluster network, were examined to determine the optimal number of client, or slave, nodes for each server, or master, node. The optimal number of clients per server was determined to be eight. More clients per server degraded overall performance due to increased communication between machines and fewer clients per server resulted in underutilization of the system. By combining the client and server activities on a single machine using a virtual server setup, four different base T fields could be calibrated simultaneously on the 32 machines.

TFIELD-7.0 T-FIELD ACCEPTANCE CRITERIA

The calibration procedure described in Section 6.0 of this attachment was applied to 150 of the base T fields (the remaining 350 base fields were held in reserve, to be used only if necessary). Not all base T fields yielded a resulting calibrated T field. Four base T fields (d01r03, d01r09, d02r09, and d08r10) encountered numerical difficulties during the first iteration and did not calibrate at all. For each of the remaining 146 T fields, the calibration procedure stopped for one of three reasons:

1. PEST completed the maximum allowed number of iterations (15);
2. PEST was unable to improve the objective function (sum of squared errors of weighted residuals) for three successive iterations; or
3. the optimization became numerically unstable.

Some of the T fields probably could have been calibrated better with more effort and adjustment of some of the PEST input parameters; however, these parameters were set to work across the largest number of fields possible and no calibration process will necessarily be able to make progress on every base field given the same set of parameters.

Because the T-field calibration procedure did not stop when some objective goodness-of-fit target was achieved, criteria had to be established to define what constitutes an acceptable calibration for use in the WIPP CRA calculations. Because the T fields were to be used for calculation of radionuclide transport, the travel times calculated in the T fields for a conservative particle released above the center of the WIPP waste panels (UTM X = 613,597.5 m and Y = 3,581,385.2 m [Ramsey et al. 1996, p. 9]) to reach the WIPP land-withdrawal boundary (LWB) were used in developing acceptance criteria. That is, the sensitivity of the calculated travel-time distribution to potential acceptance criteria was used to identify those criteria that are important. Once the distribution of travel times showed no (remaining) sensitivity to continued refinement of the criteria applied (e.g., a reduction in some metric below a threshold value), all T fields meeting those criteria were considered to be acceptably calibrated.

The travel times discussed herein were obtained using the streamline particle-tracking algorithm implemented in DTRKMF v. 1.0 (Rudeen 2003) assuming a single-porosity medium with a porosity of 0.16. DTRKMF calculates particle tracks in two or three dimensions for steady-state and time-dependent, variably saturated flow fields. The particles are tracked cell-by-cell using a semi-analytical solution. DTRKMF assumes that the velocities vary linearly between the cell faces as a function of the space coordinate and, for time-dependent cases, that the velocities at the faces vary linearly between time planes. It directly reads the cell-by-cell flow budget file from MODFLOW-2000 and uses those values to calculate the velocity field. For each calibrated T field, a final forward run of MODFLOW-2000 was done and the cell-by-cell fluxes from this run were used as input to DTRKMF to calculate the travel time. For each calibrated T field, only a single particle was tracked, providing a single travel time. The MODFLOW-2000 modeling was performed using a 7.75-m (25.4-ft) thickness for the Culebra, whereas transport calculations assume that all flow is concentrated in the lower 4.0 m (13 ft) of Culebra (Meigs and McCord, 1996). Therefore, the travel times obtained from DTRKMF were scaled by multiplying by the

1 factor 0.516 (4/7.75). These scaled travel times were then consistent with the travel times
 2 calculated and reported by Wallace (1996) for the T fields used in the WIPP CCA (DOE 1996).
 3 These travel times do not, however, represent the actual predicted travel times of solutes,
 4 conservative or non-conservative, through the Culebra. Culebra transport modeling treats the
 5 Culebra as a double-porosity medium with transport through advective porosity (e.g., fractures)
 6 retarded by diffusion into diffusive porosity (e.g., matrix porosity) and by sorption. The travel
 7 times presented herein are intended only to allow comparison among T fields.

8 ***TFIELD-7.1 Candidate Acceptance Criteria***

9 Four factors were evaluated for their potential to provide T-field acceptance criteria: the root
 10 mean squared error (RMSE) of the modeled fit to the measured steady-state heads, the agreement
 11 between the measured and modeled steady-state gradient/heads, the sum of squared weighted
 12 residuals (ϕ) for the transient data, and the agreement between the measured and modeled
 13 transient heads. These factors are not totally independent of one another, but are related in ways
 14 discussed below.

15 ***TFIELD-7.1.1 RMSE Values***

16 The RMSE is a measure of how close MODFLOW-2000/PEST came to matching the measured
 17 steady-state heads for each T field. The RMSE is defined as:

$$18 \quad RMSE = \sqrt{\frac{\sum_{i=1}^{n_{obs}} (H_i^{obs} - H_i^{calc})^2}{n_{obs}}} \quad (10)$$

19 where n_{obs} is the number of head observations and H^{obs} and H^{calc} are the values of the observed
 20 and calculated heads, respectively. Previous Culebra T-field calibration exercises (e.g., LaVenue
 21 and RamaRao 1992) achieved RMSEs less than 3 m (9.5 ft) in most cases when calibration was
 22 being performed only to steady-state heads. This level of calibration was also achieved by
 23 McKenna and Hart (2003a) for four different sets of steady-state head measurements. RMSEs
 24 have not previously been reported for steady-state heads in Culebra T fields calibrated to
 25 transient heads.

26 ***TFIELD-7.1.2 Fit to Steady-State Heads***

27 One measure of how well a T field has matched the steady-state heads can be obtained by simply
 28 plotting the measured heads versus the modeled heads. If the measured and modeled heads
 29 match exactly, the best-fit straight line through the data will have a slope of one. Exact
 30 agreement between measured and modeled heads is not to be expected, so an acceptance
 31 criterion on the slope of the best-fit line must be established.

32 The steady-state heads are important because the transport calculations performed in
 33 SECOTP2D rely on the steady-state velocity field provided by MODFLOW-2000. If
 34 MODFLOW-2000 has not accurately captured the steady-state heads, steady-state gradients and
 35 the associated steady-state velocities will be in error. With measured head plotted as the
 36 independent variable (x) and calculated head plotted as the dependent variable (y), a slope of the

1 best-fit line less than unity implies that the calculated gradient is less than the measured gradient.
2 Low gradients should lead to excessively long travel times. Therefore, it was important to
3 determine if a threshold value of the steady-state-fit slope exists above which the distribution of
4 travel times is insensitive.

5 ***TFIELD-7.1.3 Phi Values***

6 As shown in Equation (9), phi values have three components:

- 7 • A weighted sum of squared residuals for the steady-state heads,
- 8 • A weighted sum of squared residuals for the transient drawdowns, and
- 9 • A weighted sum of squared differences between T values for each pair of pilot points.

10 The steady-state component of phi is a weighted, squared, and summed expression of the RMSE
11 given in Equation (10), above, and is not, therefore, meaningful to consider when RMSE is
12 already being considered. The pilot-point-regularization component of phi relates to the
13 smoothness of the T field, not to the goodness of fit of the measured and modeled responses.
14 Hence, only the transient component of phi is considered in the discussion that follows.

15 For reasons discussed in Section 6.7 of this attachment, transient phi values do not provide a
16 completely unbiased measure of how well a calibrated T field represents the actual T field.
17 “Measurements” of zero drawdown were given arbitrarily high weights in the calibration
18 process, the number of measurements used from individual wells during individual tests and the
19 number of measurements used from all wells during a single test varied, and some parts of the
20 modeling domain are covered by multiple wells’ responses, while other parts of the domain have
21 no transient response data. Therefore, no simple numerical value can be established that
22 represents an average residual of some meaningful value for each transient measurement, such as
23 the RMSE used to evaluate T-field calibration to steady-state heads alone. Nevertheless, the
24 transient phi values do provide an indication of how well a T field met the calibration targets as
25 defined and could be used qualitatively to define acceptable T fields.

26 ***TFIELD-7.1.4 Fit to Transient Heads***

27 Evaluating the model match to transient heads is not as straightforward as for the steady-state
28 heads because the transient match involves both the magnitude and the timing of head changes.
29 The magnitude and timing of a transient response are governed by both the transmissivity and
30 storativity (S) of a system, but S was not included as a calibration parameter during the
31 calibration process. A single S value of 1×10^{-5} ($\log_{10} = -5$) was used during T-field calibration.
32 As reported by Beauheim (2003a), the apparent storativities obtained from independent analyses
33 of the test responses used for the calibration range from 5.1×10^{-6} ($\log_{10} = -5.29$) to 7.3×10^{-5}
34 ($\log_{10} = -4.14$). Because the calibration method only allowed PEST to adjust T to try to match
35 the measured heads, it might actually shift T away from the correct value in trying to compensate
36 for an inappropriate value of S. Thus, some allowance needed to be made for how close PEST
37 could actually come to matching the measured responses.

1 To establish the bounds of what might be considered acceptable matches to the transient heads, a
 2 series of well-test simulations using the code nSIGHTS (Roberts 2002) was performed. For
 3 base-case parameter values, a T of 1×10^{-5} m²/s and an S of 1×10^{-5} were used. Pumping in a
 4 well was simulated for 5, 25, and/or 50 days, and the responses that would be observed in
 5 observations wells 1, 2, and/or 3 km away were calculated. T and/or S were also varied by
 6 approximately a half order of magnitude upward and downward (3×10^{-5} and 3×10^{-6}). The
 7 results of these simulations are shown in Appendix A of Beauheim (2003b).

8 Based on the simulations, a set of guidelines was developed to determine if a modeled response
 9 matched a measured response within a half order of magnitude uncertainty in T and/or S. The
 10 guidelines were structured around the position of the modeled maximum drawdown relative to
 11 the measured maximum drawdown on a linear-linear plot of elapsed time on the x-axis and
 12 drawdown (increasing upward) on the y-axis. The guidelines are as follows:

- 13 • If the modeled peak occurs early and high (relative to the measured peak), S is too low
 14 and the maximum modeled drawdown can be up to three times greater than the maximum
 15 measured drawdown.
- 16 • If the modeled peak occurs early and low, T is too high and the maximum modeled
 17 drawdown can be up to two times lower than the maximum measured drawdown.
- 18 • If the modeled peak occurs late and high, T is too low and the maximum modeled
 19 drawdown can be up to two times higher than the maximum measured drawdown.
- 20 • If the modeled peak occurs late and low, S is too high and the maximum modeled
 21 drawdown can be up to three times lower than the maximum measured drawdown.
- 22 • If the modeled peak occurs at the same time as the measured peak but is high, the
 23 diffusivity (T/S) is correct, but both values are too low and the maximum modeled
 24 drawdown can be up to three times greater than the maximum measured drawdown.
- 25 • If the modeled peak occurs at the same time as the measured peak but is low, the
 26 diffusivity (T/S) is correct, but both values are too high and the maximum modeled
 27 drawdown can be up to three times lower than the maximum measured drawdown.

28 No quantitative criteria were established for how much earlier or later modeled peaks could
 29 occur relative to measured peaks because of the wide range observed in the simple scoping
 30 calculations (calculated peaks occurring a factor of 5 sooner to a factor of 10 later than the
 31 observed peaks) and because of the variability in pumping durations and distances to observation
 32 wells associated with the measured responses.

33 Using these guidelines, plots of each of the 40 transient well responses of each calibrated T field
 34 were evaluated visually to determine if the T field represented that response within a half order
 35 of magnitude uncertainty in T and/or S. A threshold number of well responses that failed this
 36 test was then considered as a possible acceptance criterion for the T fields.

1 ***TFIELD-7.2 Application of Criteria to T Fields***

2 The four criteria described above were applied to the calibrated Culebra T fields to determine if
3 they allowed meaningful discrimination among the fields. Given that travel time is the
4 performance measure of most concern, the four criteria were evaluated in terms of their effects
5 on the calculated distribution of travel times from the T fields.

6 ***TFIELD-7.2.1 RMSE Values***

7 Steady-state RMSE values for the 146 completed T fields are plotted in Figure TFIELD-44. The
8 data for H-9b, the southernmost well, were excluded from the RMSE calculation because the
9 southern model boundary condition consistently caused the modeled H-9b head to be
10 significantly lower than the measured head, disproportionately affecting the calculation of the
11 RMSE. The exclusion of the H-9b data should provide a better measure of the accuracy of the
12 model in the rest of the model domain.

13 All nine RMSE values greater than 20 m (66 ft) correspond to T fields that were not considered
14 to have been successfully calibrated by McKenna and Hart (2003b). Figure TFIELD-45 shows
15 the RMSE values plotted against travel time, and shows that the high RMSE values tend to be
16 associated with long travel times. For RMSE values less than approximately 6 m (20 ft), travel
17 times tend to cluster below approximately 50,000 years. Applying an RMSE cutoff value of 6 m
18 (20 ft) would leave 117 T fields, with all but one having travel times less than 102,000 years
19 (Figure TFIELD-46; the outlier with a travel time of ~241,000 years, d01r06, is not shown).

20 ***TFIELD-7.2.2 Fit to Steady-State Heads***

21 Figure TFIELD-47 provides an example plot of measured steady-state heads versus modeled
22 steady-state heads for one T field, with a unit-slope line shown as a reference. For each plot of
23 steady-state heads, the slope of the best-fit line through all of the data except for the data for
24 H-9b was calculated using the Excel SLOPE function. The data for H-9b, the southernmost well,
25 were excluded from this calculation because the southern model boundary condition consistently
26 caused the modeled H-9b head to be significantly lower than the measured head. Inasmuch as
27 the gradient in the extreme southern portion of the modeling domain is unimportant with respect
28 to transport across the southern half of the WIPP site, the exclusion of the H-9b data should
29 improve the accuracy of the slope calculation in the area of interest.

30 The slopes of the best-fit lines through the measured vs. modeled steady-state heads are shown
31 plotted against travel time in Figure TFIELD-48. Steady-state-fit slopes less than 0.5 appear to
32 lead to significantly longer travel times, consistent with the low hydraulic gradients the low
33 slopes imply. Of the 116 T fields with steady-state-fit slopes greater than 0.5, all but nine have
34 travel times less than 50,000 years. Figure TFIELD-49 shows the slopes and travel times for
35 these 116 fields (the outlier with a travel time of ~241,000 years, d01r06, is not shown), and
36 indicates that travel time is not sensitive to steady-state-fit slopes above 0.5.

37 ***TFIELD-7.2.3 Phi Values***

38 Transient phi values for all the completed T fields are plotted against travel time in Figure
39 TFIELD-50. As phi values decrease, particularly as they get below approximately 5,000 m²

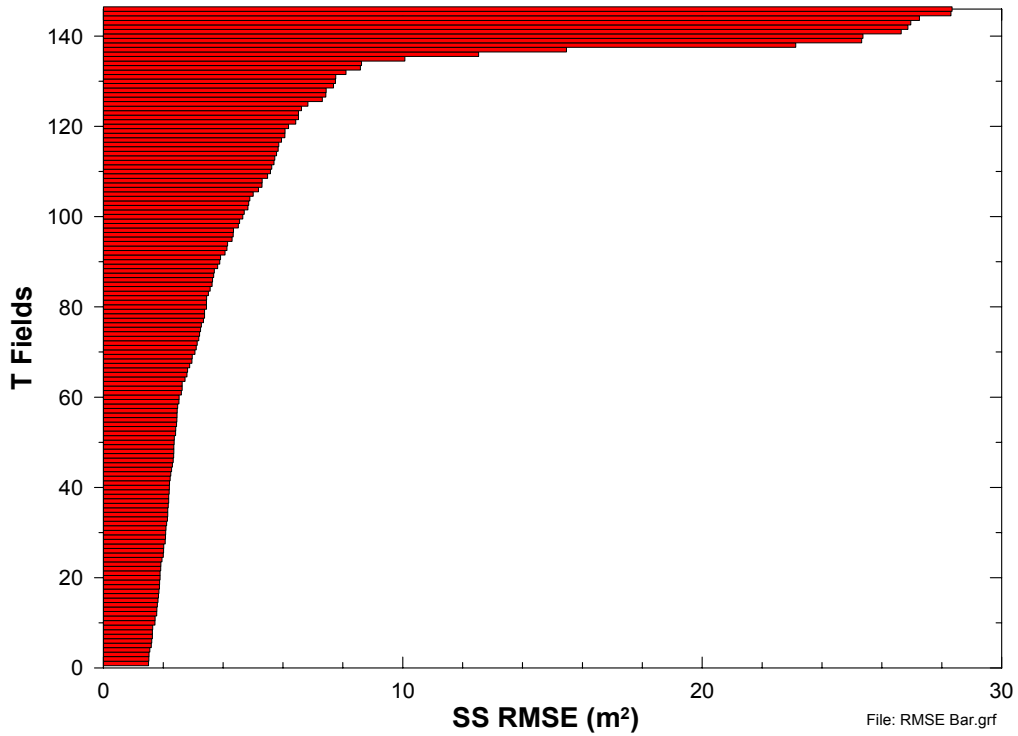


Figure TFIELD-44. Steady-State RMSE Values for 146 T Fields

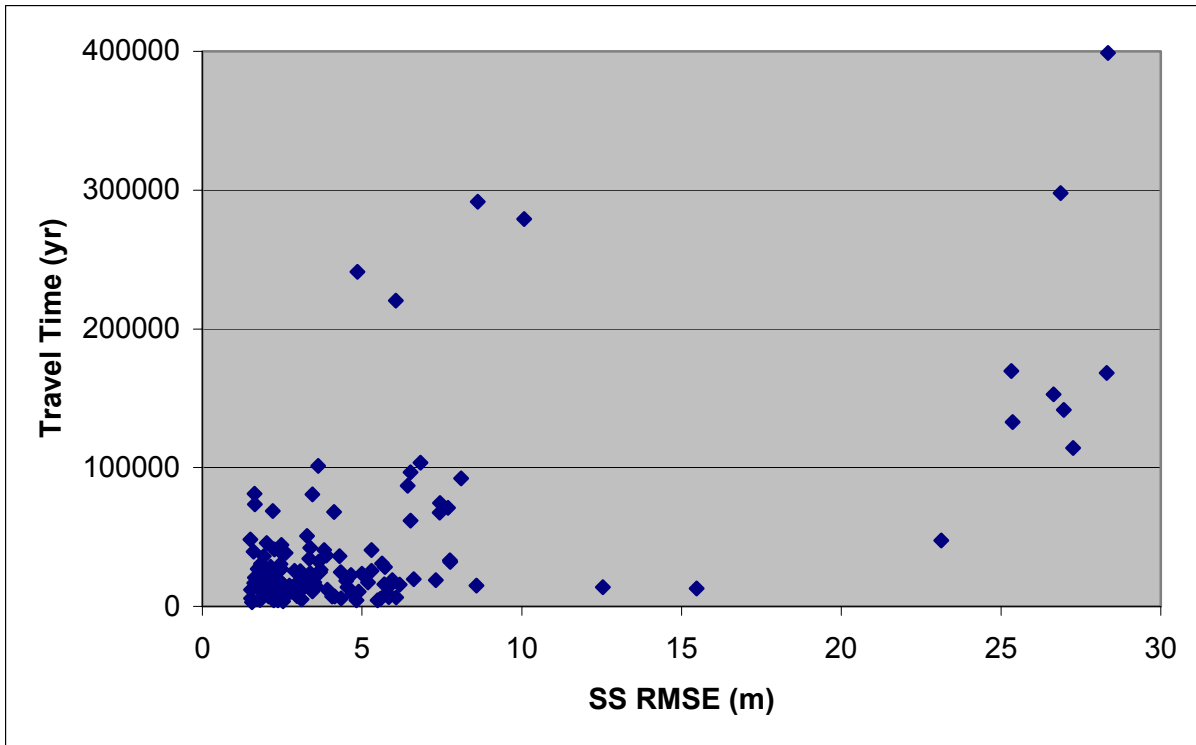
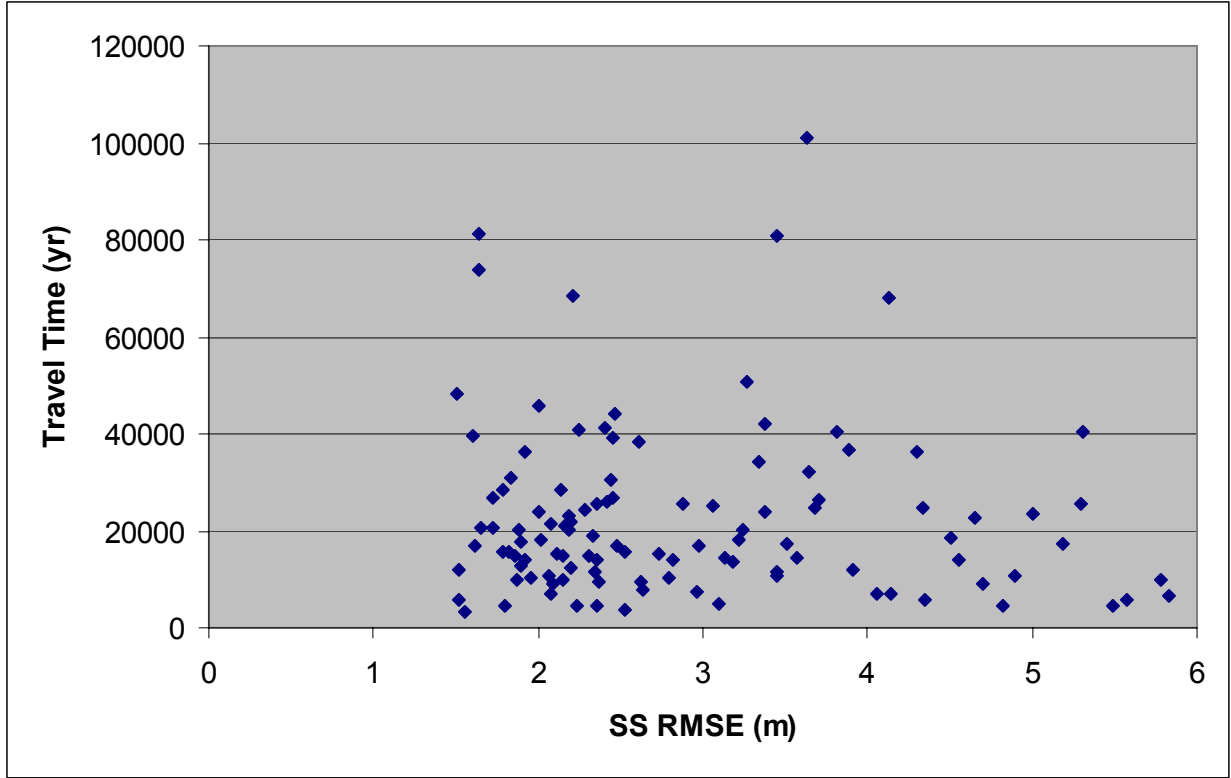


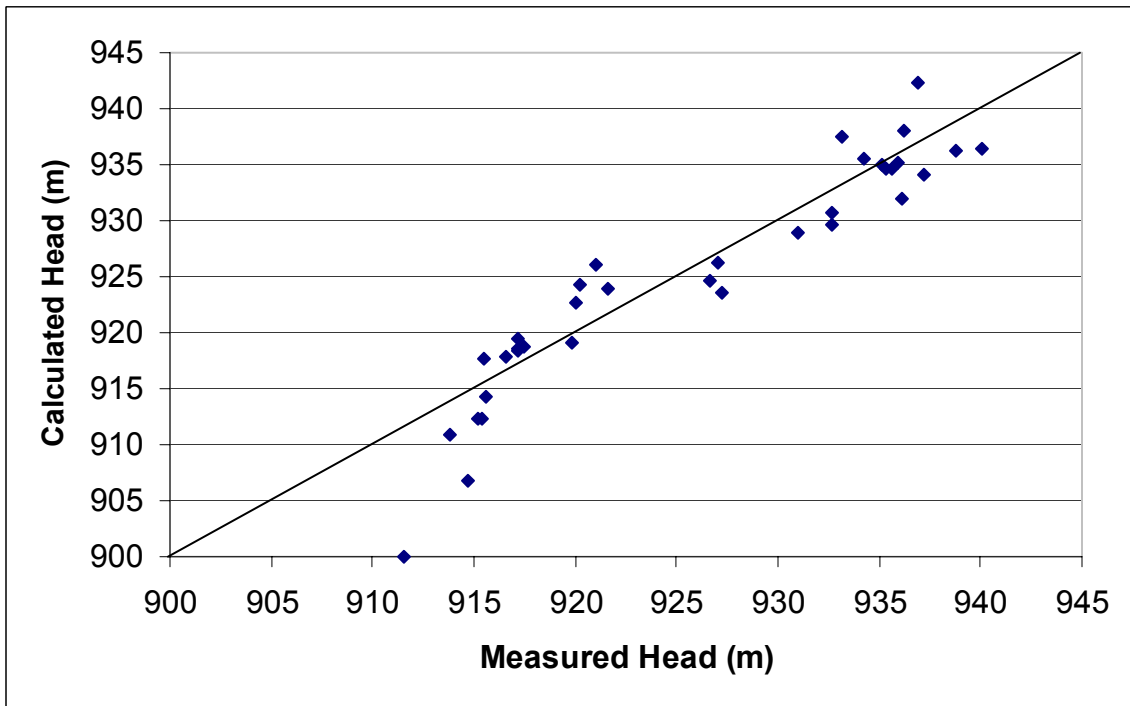
Figure TFIELD-45. Steady-State RMSE Values and Associated Travel Times



1

2

Figure TFIELD-46. Travel Times for Fields with Steady-State RMSE <6 m (20 ft)



3

4

5

Figure TFIELD-47. Measured Versus Modeled Steady-State Heads for T Field d21r10

1 (53,800 ft²), travel times tend to cluster below approximately 50,000 years, but little correlation
2 is seen between transient phi and travel time. Figure TFIELD-51 shows transient phi versus
3 travel time for the 123 fields with transient phi values less than 8,000 m² (86,000 ft²), excluding
4 the five outliers that have travel times greater than 168,000 years. This plot suggests that despite
5 the clustering of travel times below 50,000 years, the overall range of travel times does not
6 decrease significantly as phi decreases. Thus, transient phi does not appear to provide an
7 effective tool for distinguishing among T fields.

8 ***TFIELD-7.2.4 Fit to Transient Heads***

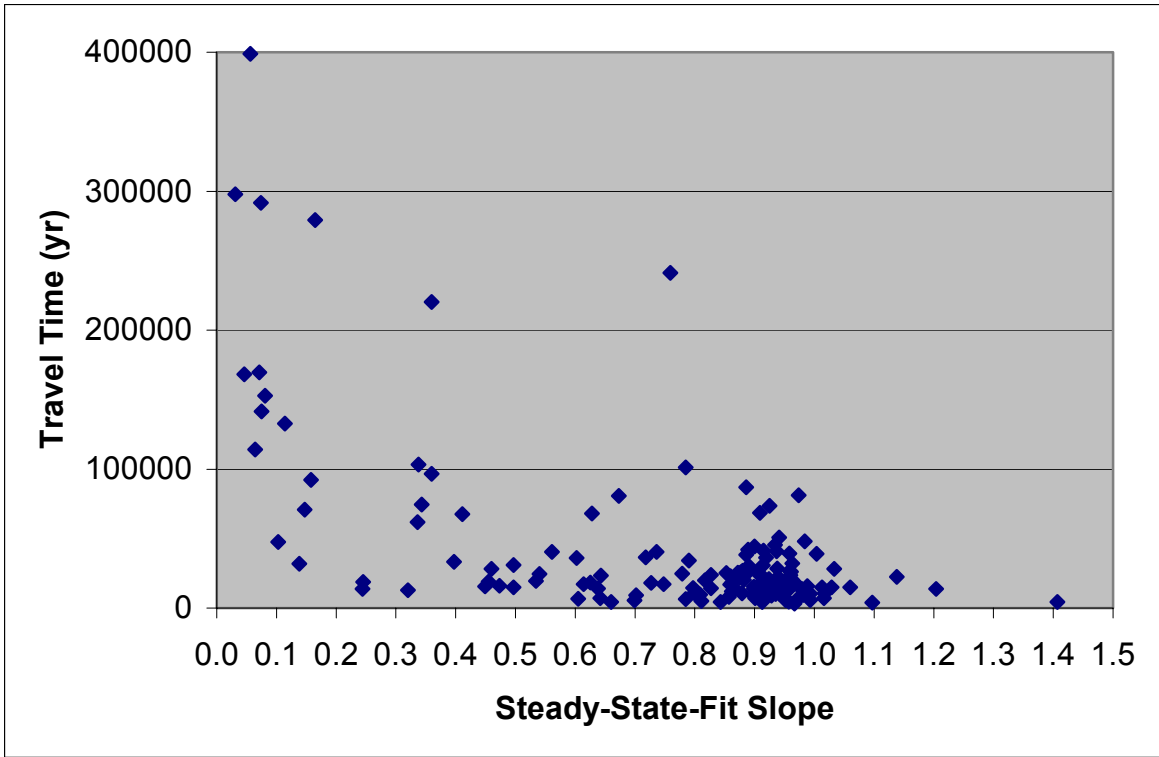
9 In applying the tests described in Section 7.1.4 of this attachment to the well responses simulated
10 for each T field, it was found that insufficient data (only six measurements) had been included
11 for the WQSP-1 response to pumping at WQSP-2 to allow any determination of model
12 adequacy. Thus, this response was eliminated from consideration for all T fields. Figures
13 TFIELD-52 and TFIELD-53 provide examples from T field d21r10 of well responses that were
14 judged to PASS and FAIL, respectively, the criteria outlined in Section 7.1.4 of this attachment.
15 The number of responses that failed for each T field is given in Table TFIELD-11. For the
16 WQSP-3 responses to pumping at WQSP-1 and WQSP-2 (for which no clear drawdown was
17 observed and “measured” values of zero were entered), the modeled response was accepted if it
18 showed no more than 0.25 m (0.82 ft) of drawdown.

19 The number of well responses that fail the tests described in Section 7.1.3 of this attachment
20 should be related to the transient phi for each T field because both are measures of the match
21 between the measured and modeled transient heads. Figure TFIELD-54 shows a plot of transient
22 phi versus the number of failed well responses for all 146 T fields. A definite correlation is
23 evident up to a phi of approximately 8,000 m² (86,000 ft²). Beyond that value, the number of
24 failed well responses simply remains high (≥ 14).

25 The number of failed well responses is plotted against travel time in Figure TFIELD-55 for each
26 of the T fields. The scatter in travel time appears to increase with 14 or more failures, but the
27 majority of T fields still have travel times in the same range as the fields with less than 14
28 failures. Thus, the number of failed well responses alone does not appear to discriminate well
29 among T fields.

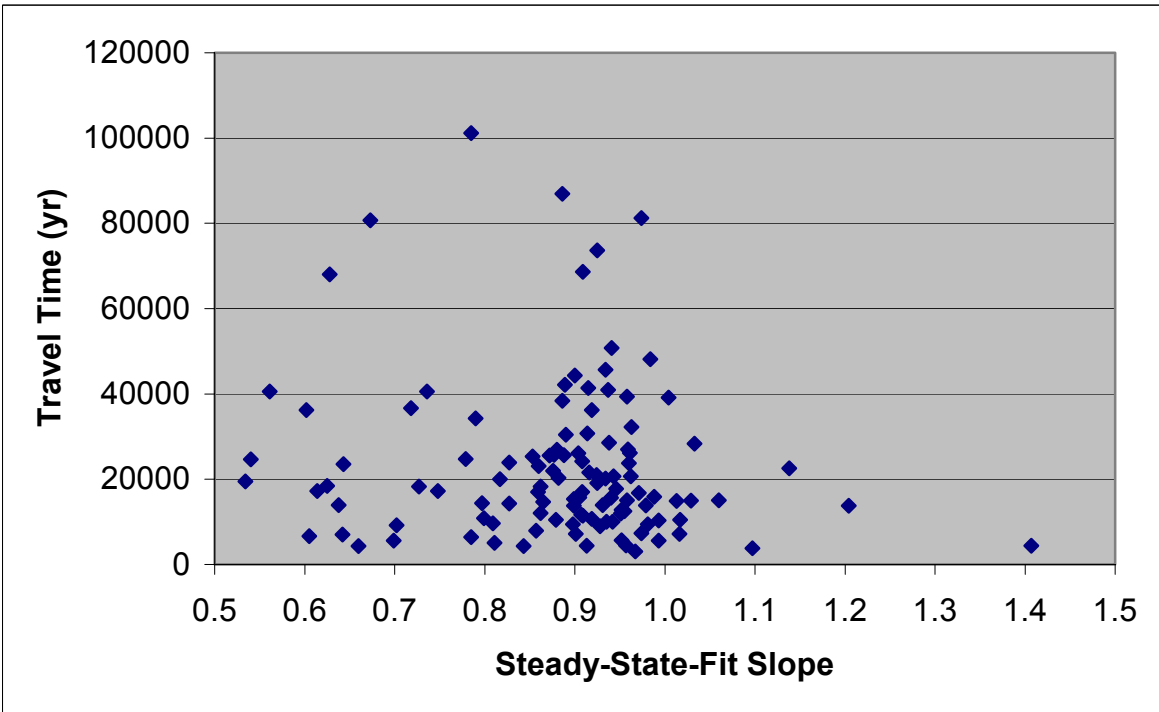
30 ***TFIELD-7.3 Final Acceptance Criteria***

31 Of the criteria discussed above, the two related to the steady-state heads (RMSE and steady-
32 state-fit slope) appear to be more effective at identifying poorly calibrated T fields than the two
33 related to transient heads (transient phi and number of failed well responses). The range and
34 scatter of travel times appears to increase at RMSE values beyond 6 m (20 ft). Applying an
35 RMSE cutoff of 6 m (20 ft) leaves 117 T fields, all with travel times less than 102,000 years
36 except one (d01r06). This cutoff also excludes all T fields with steady-state-fit slopes less than
37 0.45. Steady-state-fit slopes less than approximately 0.5 appear to lead to significantly longer
38 travel times, consistent with the low hydraulic gradients the low slopes imply. If a simple cutoff
39 of a minimum steady-state-fit slope of 0.5 is applied, 116 T fields are left, again with travel times
40 less than 102,000 years (except d01r06), and also with RMSE values less than 8.6 m (28.2 ft).
41 Five T fields that meet the RMSE less than 6 m (20 ft) criterion fail the steady-state-fit slope



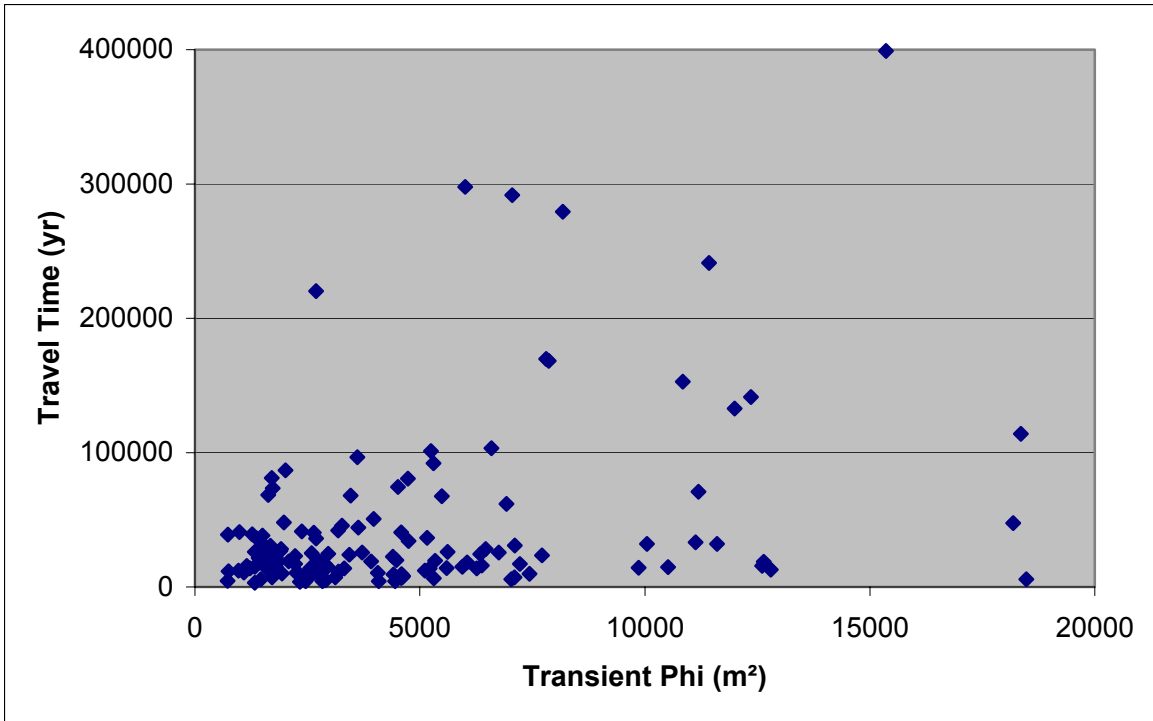
1
2

Figure TFIELD-48. Steady-State-Fit Slope Versus Travel Time for All Fields



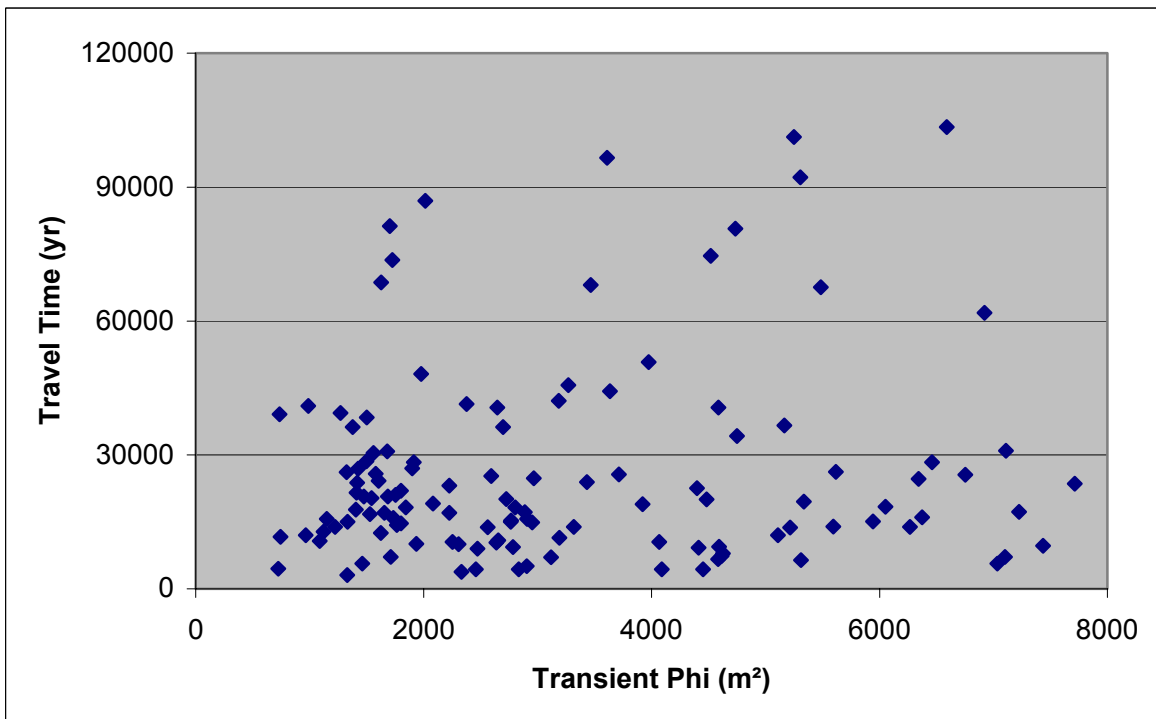
3
4

Figure TFIELD-49. Steady-State-Fit Slope Versus Travel Time for Slopes >0.5



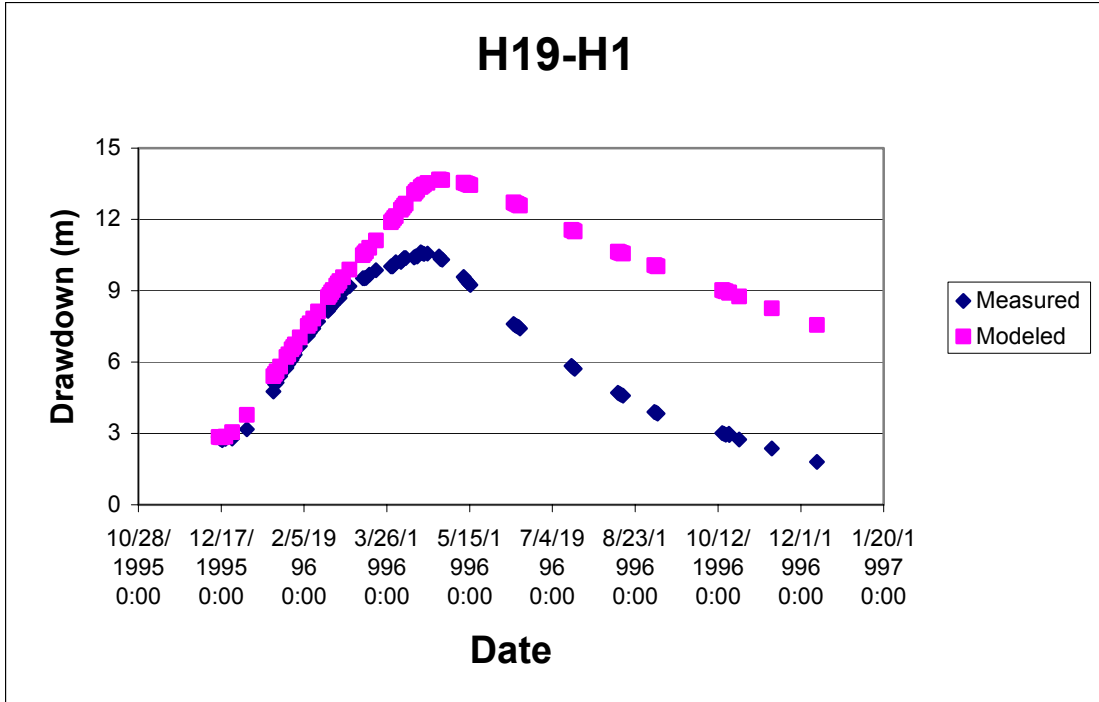
1
2

Figure TFIELD-50. Transient Phi Versus Travel Time for All Fields



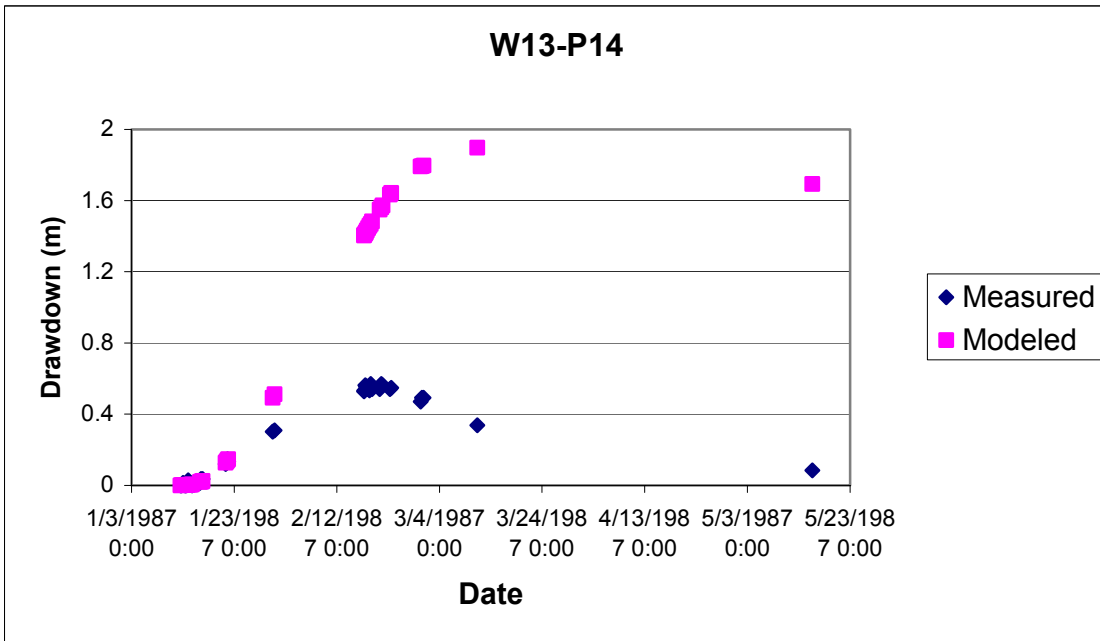
3
4
5

Figure TFIELD-51. Transient Phi Versus Travel Time for Phi <8,000 m²



1
2
3

Figure TFIELD-52. Example of Passing Well Response from T Field d21r10



4
5

Figure TFIELD-53. Example of Failing Well Response from T Field d21r10

Table TFIELD-11. Summary Information on T Fields

T Field	SS RMSE (m)	SS Phi (m²)	Transient Phi (m²)	Steady-State-Fit Slope	# of Failed Well Responses	Time to WIPP boundary (yr)
d01r01	7.427	10498	5486	0.411	13	67578
d01r02	3.915	3621	5110	0.862	20	12045
d01r04	2.812	2140	2563	1.204	11	13821
d01r05	7.313	10245	12643	0.245	16	18886
d01r06	4.856	5006	11426	0.759	15	241211
d01r07	3.377	2851	3187	0.889	9	42123
d01r08	5.484	6122	4091	1.407	14	4399
d01r10	1.646	1094	1476	0.943	9	20685
d02r01	26.966	128711	12359	0.075	19	141516
d02r02	3.507	2772	2889	0.748	11	17217
d02r03	10.070	18606	8173	0.165	15	279242
d02r04	8.104	12482	5305	0.158	12	92235
d02r05	5.184	5577	7224	0.614	17	17255
d02r06	25.325	113652	7810	0.071	16	169677
d02r07	3.648	3223	10047	0.963	15	32231
d02r08	5.001	5125	7713	0.643	17	23571
d02r10	6.066	6849	5312	0.785	13	6433
d03r01	4.506	4022	6053	0.625	17	18435
d03r02	28.346	142152	15357	0.056	16	398937
d03r03	4.146	3899	7102	1.016	17	7171
d03r04	25.367	114006	11991	0.114	14	132833
d03r05	5.836	6873	4585	0.605	13	6638
d03r06	1.729	1208	1899	0.959	13	27006
d03r07	4.655	4740	4399	1.138	13	22599
d03r08	4.550	4250	5593	0.638	17	13942
d03r09	2.352	1574	1580	0.877	7	25757
d03r10	8.584	13811	2766	1.060	13	15054
d04r01	3.447	2370	4736	0.673	17	80690
d04r02	3.818	3175	2647	0.736	12	40593
d04r03	2.352	1659	3317	0.979	12	13888
d04r04	4.298	3692	2697	0.602	13	36245
d04r05	1.507	1059	1980	0.984	9	48168
d04r06	3.705	3146	5618	0.961	16	26199
d04r07	2.183	1397	2226	0.860	10	23105
d04r08	2.444	1759	1560	0.890	11	30470
d04r09	27.256	131491	18356	0.064	16	114087
d04r10	3.060	2401	2593	0.853	9	25316
d05r01	6.427	8119	2015	0.886	13	86924
d05r02	5.298	5831	6755	0.872	16	25610
d05r03	3.444	2580	2655	0.799	11	10880
d05r04	5.862	6984	10518	0.497	17	14856
d05r05	4.346	4226	18478	0.952	16	5668
d05r06	6.518	8198	3609	0.360	13	96589
d05r07	3.188	2682	5216	0.899	9	13766
d05r08	7.686	11242	11194	0.147	16	70896
d05r09	26.644	125685	10840	0.081	17	152818
d05r10	5.623	6497	7110	0.497	16	30955
d06r01	6.828	9057	6592	0.338	17	103442
d06r02	1.957	1266	2639	0.993	9	10353
d06r03	1.637	1051	1703	0.974	10	81258
d06r04	3.214	2246	2805	0.727	13	18294

1

Table TFIELD-11. Summary Information on T Fields — Continued

T Field	SS RMSE (m)	SS Phi (m ²)	Transient Phi (m ²)	Steady-State-Fit Slope	# of Failed Well Responses	Time to WIPP boundary (yr)
<i>d06r05</i>	3.886	3516	5164	0.718	18	36644
<i>d06r06</i>	2.149	1254	2954	1.013	10	14935
<i>d06r07</i>	1.518	784	965	0.951	7	12035
<i>d06r08</i>	7.440	10397	4518	0.343	18	74565
<i>d06r09</i>	28.309	141764	7864	0.046	18	168281
<i>d06r10</i>	2.196	1455	1801	0.876	11	21990
<i>d07r01</i>	3.101	2326	2905	0.811	14	5082
<i>d07r02</i>	2.010	1327	3271	0.934	15	45647
<i>d07r03</i>	15.470	42986	12795	0.320	19	12919
<i>d07r04</i>	5.579	6230	7033	0.699	18	5638
<i>d07r05</i>	2.727	1705	5942	0.958	10	15097
<i>d07r06</i>	4.334	3927	6345	0.540	12	24641
<i>d07r07</i>	2.477	1737	2225	0.908	9	17038
<i>d07r08</i>	2.232	1097	2836	0.843	9	4355
<i>d07r09</i>	2.207	1239	1628	0.909	8	68629
<i>d07r10</i>	1.782	839	1150	0.940	9	15680
<i>d08r01</i>	2.361	1736	2458	0.913	11	4388
<i>d08r02</i>	2.418	1168	1326	0.904	6	26115
<i>d08r03</i>	2.137	1489	1499	0.938	9	28570
<i>d08r04</i>	3.683	2674	2966	0.779	9	24773
<i>d08r05</i>	2.115	1384	2769	0.899	13	15358
<i>d08r06</i>	1.916	1388	1225	0.931	11	13917
<i>d08r07</i>	1.857	815	1333	1.029	10	15027
<i>d08r08</i>	12.534	28547	6267	0.244	12	13885
<i>d08r09</i>	5.785	6674	7437	0.809	17	9691
<i>d09r01</i>	8.621	13909	7050	0.074	11	291623
<i>d09r02</i>	3.243	2418	4482	0.817	12	20048
<i>d09r03</i>	2.252	1337	989	0.937	8	40948
<i>d09r04</i>	1.892	710	1123	0.952	8	12857
<i>d09r05</i>	2.061	954	1088	0.919	8	10726
<i>d09r06</i>	2.794	2313	2253	0.879	16	10509
<i>d09r07</i>	2.629	1676	4591	0.981	10	9472
<i>d09r08</i>	1.895	1030	1406	0.946	9	17741
<i>d09r09</i>	4.826	4945	4453	0.660	14	4359
<i>d09r10</i>	3.273	2790	3976	0.941	19	50791
<i>d10r01</i>	26.867	127794	6006	0.031	14	297840
<i>d10r02</i>	1.554	589	1330	0.967	8	3111
<i>d10r03</i>	2.201	1474	1626	0.955	9	12533
<i>d10r04</i>	2.527	1788	2334	1.097	9	3799
<i>d10r05</i>	5.722	6646	6463	0.460	18	28390
<i>d10r06</i>	4.702	4644	4412	0.702	13	9210
<i>d10r07</i>	1.870	810	1937	0.935	10	10068
<i>d10r08</i>	2.334	1613	2083	0.925	8	19093
<i>d10r09</i>	4.128	3643	3466	0.628	11	68052
<i>d10r10</i>	1.789	982	1915	1.033	13	28367
<i>d11r01</i>	2.970	2297	1655	0.859	9	17015
<i>d11r02</i>	2.308	1799	1801	0.865	12	14677
<i>d11r03</i>	5.700	6093	6376	0.473	9	16014
<i>d11r04</i>	6.514	8401	6922	0.336	23	61862
<i>d11r05</i>	5.952	7166	3921	0.455	17	18998
<i>d11r06</i>	2.607	1949	1503	0.886	9	38399

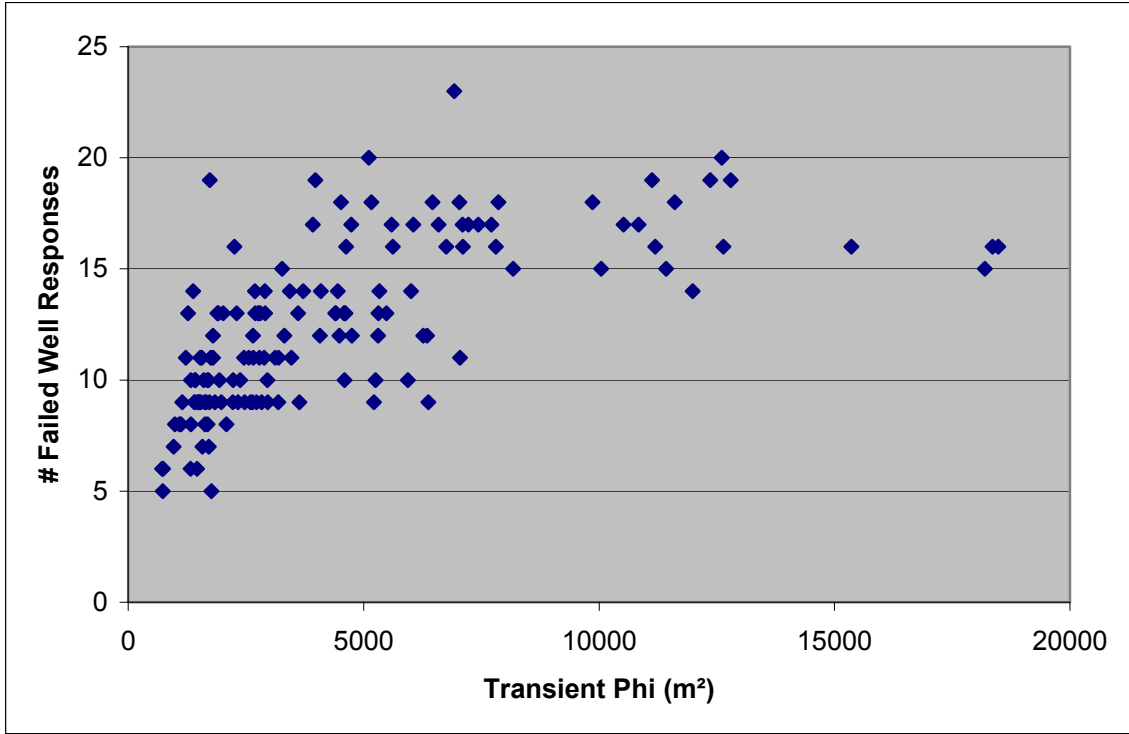
Table TFIELD-11. Summary Information on T Fields — Continued

T Field	SS RMSE (m)	SS Phi (m ²)	Transient Phi (m ²)	Steady-State-Fit Slope	# of Failed Well Responses	Time to WIPP boundary (yr)
<i>d11r07</i>	1.639	602	1727	0.925	9	73634
<i>d11r08</i>	1.801	1206	723	0.957	6	4520
<i>d11r09</i>	2.073	858	1712	0.901	7	7199
<i>d11r10</i>	3.135	2363	1767	0.827	5	14358
<i>d12r01</i>	3.378	2921	3432	0.827	14	23936
<i>d12r02</i>	2.459	1795	1426	0.880	10	26919
<i>d12r03</i>	1.618	558	1530	0.971	11	16780
d12r04	6.182	7395	12605	0.449	20	15619
<i>d12r05</i>	1.522	918	1463	0.993	6	5655
<i>d12r06</i>	1.602	539	1271	0.958	13	39399
<i>d12r07</i>	2.016	945	1844	0.862	9	18283
<i>d12r08</i>	2.630	1879	4627	0.857	16	7981
<i>d12r09</i>	2.369	1671	2784	0.898	11	9414
d12r10	7.762	11431	11606	0.138	18	32059
<i>d13r01</i>	2.163	1061	1753	0.924	11	21032
<i>d13r02</i>	2.881	2054	3715	0.888	14	25639
<i>d13r03</i>	3.444	2580	3192	0.909	11	11493
<i>d13r04</i>	5.302	5856	4588	0.561	13	40601
<i>d13r05</i>	3.343	2671	4750	0.790	12	34247
<i>d13r06</i>	2.410	1441	2377	0.915	10	41400
<i>d13r07</i>	2.280	1395	1606	0.908	10	24211
<i>d13r08</i>	1.879	779	1544	0.882	9	20313
<i>d13r09</i>	1.919	776	1379	0.919	14	36260
d13r10	6.063	6685	2693	0.360	14	220354
<i>d21r01</i>	2.151	1555	2307	0.942	13	10042
<i>d21r02</i>	2.087	1431	2473	0.928	9	9023
<i>d21r03</i>	2.346	1299	744	0.907	6	11671
<i>d21r04</i>	2.523	1978	2908	0.905	13	15717
<i>d21r05</i>	2.001	932	1417	0.960	10	23750
<i>d21r06</i>	1.721	655	1688	0.962	8	20715
<i>d21r07</i>	2.182	1179	2725	0.934	9	20141
<i>d21r08</i>	6.620	8618	5337	0.534	14	19534
d21r09	7.750	11501	11124	0.397	19	33308
<i>d21r10</i>	2.959	2226	4615	0.974	13	7384
d22r01	23.126	94895	18190	0.103	15	47563
<i>d22r02</i>	3.629	3197	5250	0.785	10	101205
<i>d22r03</i>	4.061	3464	3119	0.642	11	7067
<i>d22r04</i>	4.894	5073	4068	1.017	12	10537
<i>d22r05</i>	3.566	3160	9863	0.797	18	14385
<i>d22r06</i>	2.469	1145	3635	0.900	9	44309
<i>d22r07</i>	2.080	999	1413	0.916	9	21589
<i>d22r08</i>	1.837	809	1681	0.914	10	30771
<i>d22r09</i>	1.822	724	1734	0.988	19	15870
<i>d22r10</i>	2.452	1684	735	1.004	5	39116

1
2
3
4

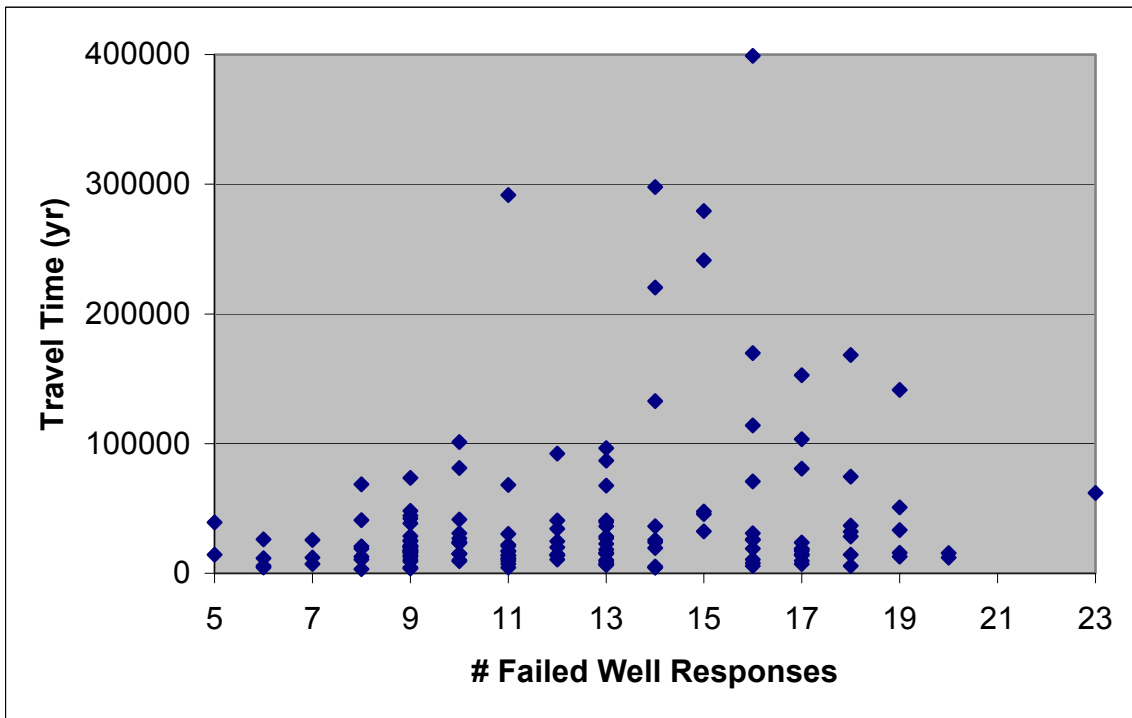
Reverse type signifies T fields not meeting final acceptance criteria.

Bold italics type signifies 100 final T fields as discussed in Section 7.3 of this attachment.



1
2

Figure TFIELD-54. Transient Phi Versus Number of Failed Well Responses

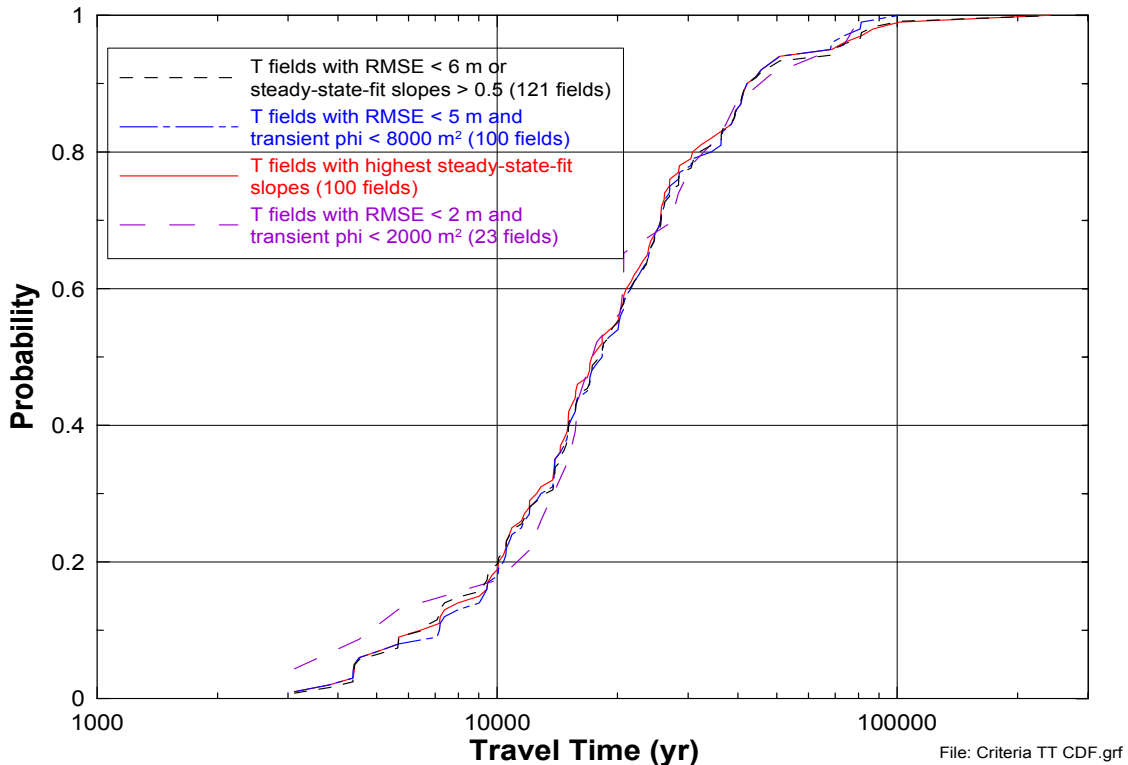


3
4

Figure TFIELD-55. Number of Failed Well Responses Versus Travel Time

1 greater than 0.5 criterion, while four T fields meeting the slope criterion fail the RMSE criterion.
 2 Thus, 112 T fields meet both criteria while 121 T fields meet at least one of the criteria.

3 Figure TFIELD-56 shows a CDF for the 121 T fields meeting the RMSE and/or steady-state-fit
 4 slope criteria discussed above. Also shown are curves representing the 100 T fields with RMSE
 5 values <5 m (16 ft) and transient phi values <8,000 m² (86,111 ft²), and the 100 T fields with the
 6 largest steady-state-fit slopes (>0.72). All three CDFs are very similar, the most significant
 7 difference being that imposing a cutoff value on transient phi eliminates the T field with the
 8 longest travel time (d01r06). To illustrate the effects of imposing more stringent constraints on
 9 T-field acceptance, a fourth CDF is shown in Figure TFIELD-56 that represents the 23 T fields



10

11 **Figure TFIELD-56. Travel-Time CDFs for Different Sets of T Fields**

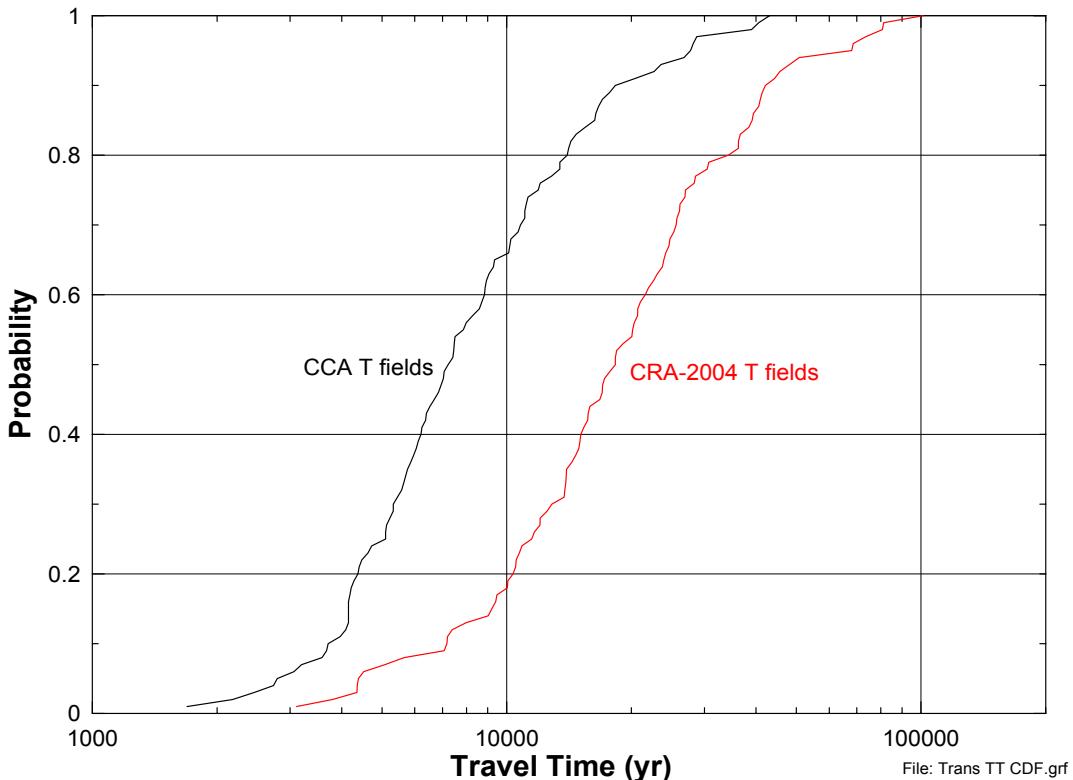
11

12 that have RMSE values less than 2 m (7 ft) and transient phi values less than 2,000 m² (21,527
 13 ft²). These 23 T fields all have steady-state-fit slopes greater than 0.88. This CDF generally
 14 shows travel times similar to those of the other CDFs, except at the tails of the distribution which
 15 are poorly defined because of the relatively small sample size. Thus, because all the CDFs
 16 shown are similar, all 121 T fields meeting the steady-state-fit slope or RMSE criteria were
 17 considered to be acceptably calibrated. The T fields that have been rejected are shown in reverse
 18 type in Table TFIELD-11.

19 Because only 100 T fields were needed, the criteria were refined to eliminate more T fields.
 20 Given that lower travel times provide a conservative (in terms of leading to increased solute
 21 transport) way to discriminate among sets of T fields, the 100 T fields with RMSE values <5 m
 22 (16 ft) and transient phi values <8,000 m² were selected for use in CRA-2004 calculations of

1 radionuclide transport through the Culebra because that set excluded the calibrated T field with
 2 the longest travel time. These T fields are highlighted in *bold italicized* type in Table
 3 TFIELD-11.

4 For comparison purposes, the CDF of travel times for these 100 T fields is plotted in Figure
 5 TFIELD-57 with the CDF of travel times for the 100 transient-calibrated T fields used in the
 6 CCA (Wallace 1996). Generally speaking, travel times are two to three times as long in the
 7 CRA-2004 fields as in the CCA fields. Considering the degree of uncertainty involved in
 8 characterizing a geologic medium on the scale of the T fields, a factor of two or three difference
 9 in travel-time CDFs represents excellent agreement.



10
 11 **Figure TFIELD-57. Travel-Time CDFs for CCA and CRA-2004 T Fields**

12 ***TFIELD-8.0 INVERSE MODELING RESULTS***

13 Some fit statistics (phi, RMSE, etc.) for the 121 T fields that were judged to be acceptably
 14 calibrated were presented in Section 7.0 of this attachment. Visualizations of the T fields are
 15 included in Annex A. Additional properties or characteristics of the T fields are given below.

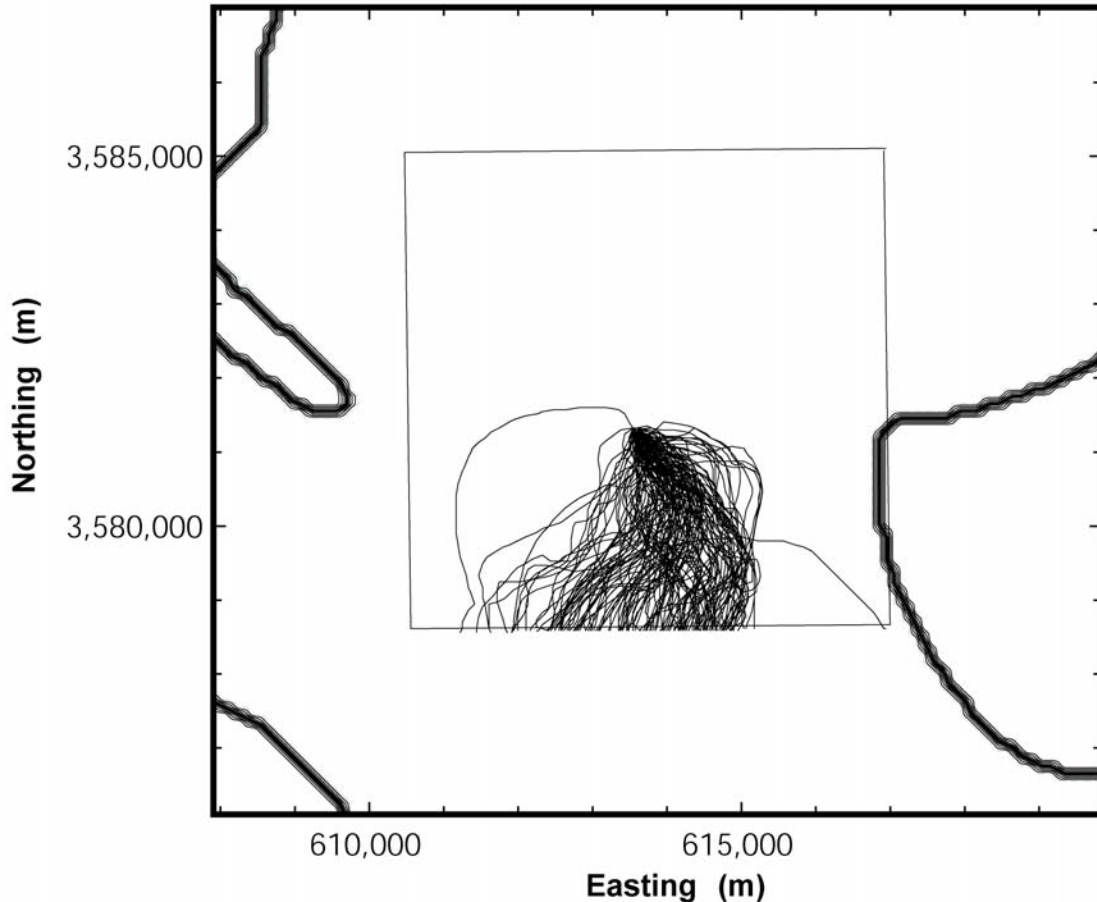
16 ***TFIELD-8.1 Particle Tracking***

17 Particle tracking was performed in the 121 calibrated T fields from a point above the center of
 18 the WIPP disposal panels to both the LWB and the boundary of the model domain, as discussed
 19 in Section 7.0 of this attachment. The locations of all the particle tracks are show in Figures
 20 TFIELD-58 and TFIELD-59. In both figures, the particle tracks are shown using only every 20th

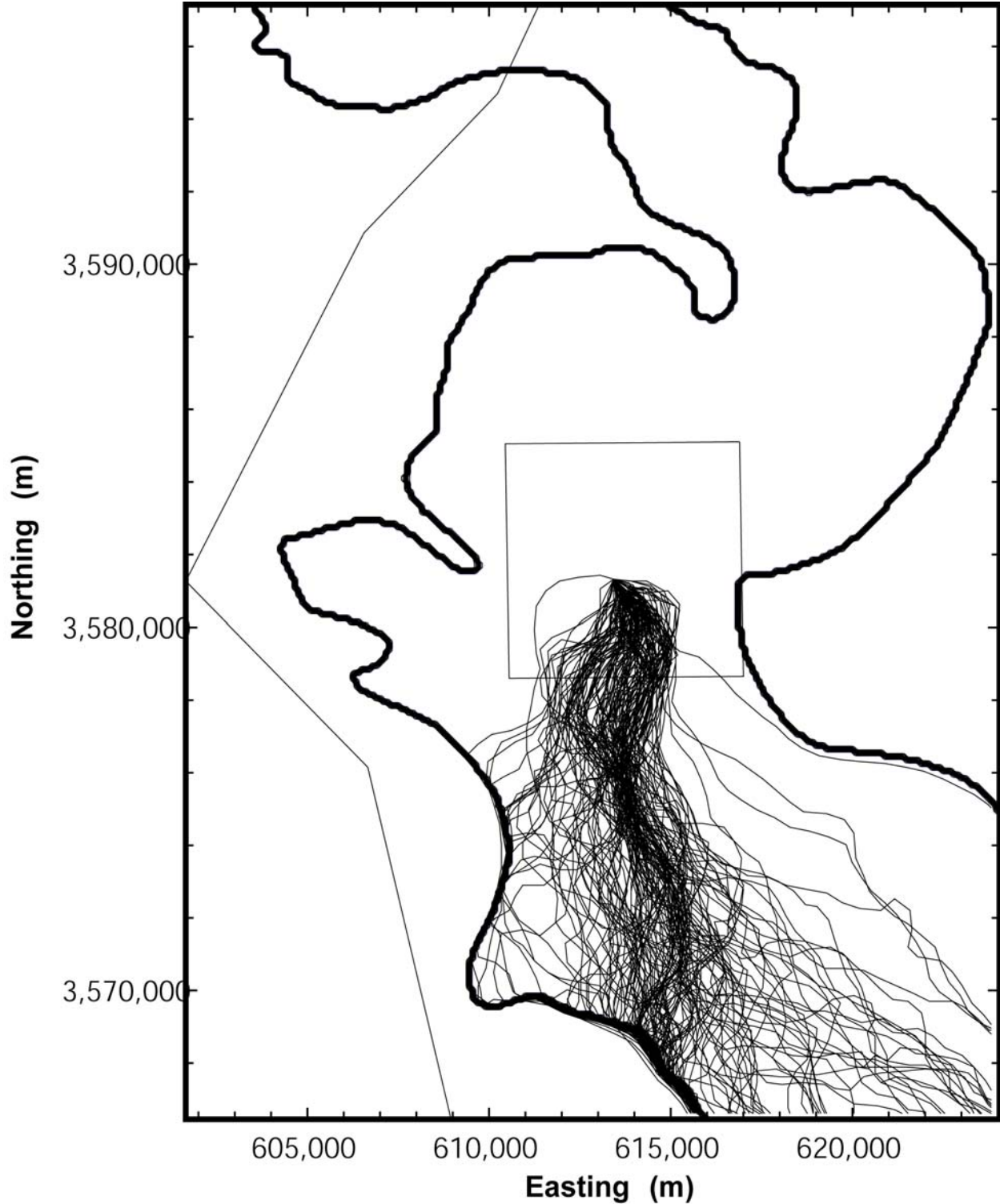
1 point along the track because of a limitation in the graphing software. This filtering leads to the
 2 particle tracks appearing less smooth than they actually are. Figure TFIELD-58 shows a close-
 3 up view of the particle tracks within the WIPP LWB. All of the particles exit the southern edge
 4 of the LWB and the majority of the particles exit the LWB to the southeast of the release point,
 5 although not as far to the east as the particle tracks for the CCA T fields showed (Ramsey et al.
 6 1996, p. 49). Figure TFIELD-59 shows the particle tracks within the entire model domain. The
 7 majority of the particles exit the domain nearly due south of the release point. The particles that
 8 migrate to the west tend to travel along the boundary of the high-T zone. This result is due to the
 9 large amount of groundwater flux within the high-T zone creating a streamline at the high-T
 10 zone boundary.

11 **TFIELD-8.2 Fit to Steady-State Heads**

12 Some information about how well the calibrated T fields matched the observed steady-state
 13 heads is given in Sections 7.2.1 and 7.2.2 of this attachment. Additional information is shown in



14
 15 **Figure TFIELD-58. All Particle Tracks Within the WIPP LWB. The bold lines show the**
 16 **boundaries of the high-T (left side) and low-T (right side) zones.**



1
2
3
4
5

Figure TFIELD-59. All Particle Tracks Within the Model Domain. The bold lines show the boundaries of the high-T (left) and low-T (right) zone boundaries. The no-flow and WIPP site boundaries are also shown.